

AdaptSFL: Adaptive Split Federated Learning in Resource-constrained Edge Networks

Zheng Lin, Guanqiao Qu, Wei Wei, Xianhao Chen, *Member, IEEE*, Kin K. Leung, *Fellow, IEEE*

Abstract—The increasing complexity of deep neural networks poses significant barriers to democratizing them to resource-limited edge devices. To address this challenge, split federated learning (SFL) has emerged as a promising solution by offloading the primary training workload to a server via model partitioning while enabling parallel training among edge devices. However, although system optimization substantially influences the performance of SFL under resource-constrained systems, the problem remains largely uncharted. In this paper, we provide a unified convergence analysis of SFL which quantifies the impact of model splitting (MS) and client-side model aggregation (MA) on its learning performance, serving as a theoretical foundation. Then, we propose AdaptSFL, a novel resource-adaptive SFL framework, to expedite SFL under resource-constrained edge computing systems. Specifically, AdaptSFL adaptively controls MS and client-side MA to balance communication-computing latency and training convergence. Extensive simulations across various datasets validate that our proposed AdaptSFL framework takes considerably less time to achieve a target accuracy than benchmarks, demonstrating the effectiveness of the proposed strategies.

Index Terms—Distributed learning, split federated learning, client-side model aggregation, model splitting, mobile edge computing.

I. INTRODUCTION

With the increasing prevalence of edge devices such as smartphones, laptops, and wearable gadgets, a vast amount of data is being generated at the network edge. It is forecasted that there will be 50 billion IoT devices, generating 79.4 Zettabytes of data in 2025 [1]. This unprecedented volume of data unlocks the potential of artificial intelligence (AI), leading to significant achievements in pivotal domains such as smart healthcare, intelligent transportation, autonomous driving, and natural language processing [2]–[6].

Most existing ML frameworks focus on centralized learning (CL), where a cloud server collects raw data from each participating device to train a powerful model. However, transferring enormous amounts of data from edge devices to the cloud server is impractical due to significant latency and bandwidth costs [7]–[11]. Moreover, clients are often reluctant to share raw data due to privacy concerns [12], which further hinders the deployment of CL. To tackle this issue, federated learning (FL) [13], [14] has been proposed as

an alternative privacy-preserving distributed ML framework. In FL, all participating devices perform model training with locally residing data in parallel and update the model by exchanging model parameters rather than raw data with a fed server. Nevertheless, the practical implementation of FL in edge networks still encounters significant challenges. As ML models scale up, on-device training for AI-driven computation-intensive tasks becomes infeasible [15]. For instance, the recently prevalent Gemini Nano-2 model, an on-device large language model, comprises 3.25 billion parameters (3GB for 32-bit floats), which is extremely challenging for on-device training as required by FL.

Split learning (SL) [16] is a promising distributed ML framework capable of overcoming the weakness of FL. Specifically, SL partitions the global model into client-side and server-side sub-models and places them on the devices and server for co-training [17], [18]. During model training, devices and the server exchange intermediate results (i.e., activations and activations' gradients) at the cut layer. This paradigm offloads the primary computing workload to a more powerful server via model splitting, significantly saving client-side computing costs. In addition, each device sends intermediate results with smaller data sizes instead of the entire ML model parameters, potentially reducing communication overhead. However, the original SL, named vanilla SL, employs a sequential training paradigm from one device to another, substantially lowering model training efficiency and leading to excessive training latency.

To address this issue, split federated learning (SFL) [19] has been proposed, amalgamating the advantages of parallel training from FL and model splitting from SL, as shown in Fig. 1. Apart from model splitting, SFL features periodic server-side and client-side sub-model aggregation to achieve model synchronization after several training rounds, following the design principle of FL. Due to its salient advantages, SFL has attracted significant attention from academia and industry in recent years. For instance, Huawei deems SFL as a key learning framework for 6G edge intelligence [20]. Nevertheless, despite its importance, the system optimization for SFL over resource-constrained systems is still in its nascent stage. In resource-constrained edge networks, the essential decisions, such as model splitting (MS) and client-side model aggregation (MA), heavily affect the model training accuracy and convergence speed. Importantly, SFL exhibits different convergence behavior compared with FL, making optimization non-trivial. This is mainly because server-side sub-models and client-side sub-models can be aggregated at varied frequencies in SFL. In particular, server-side sub-models, which are co-

Z. Lin, G. Qu, W. Wei and X. Chen are with the Department of Electrical and Electronic Engineering, University of Hong Kong, Pok Fu Lam, Hong Kong, China (e-mail: linzheng@eee.hku.hk; gqqu@eee.hku.hk; weiwei@eee.hku.hk; xchen@eee.hku.hk).

K. K. Leung is with the Electrical and Electronic Engineering Department, and the Computing Department, Imperial College, SW7 2BT London, U.K. (e-mail: kin.leung@imperial.ac.uk).

(Corresponding author: Xianhao Chen)

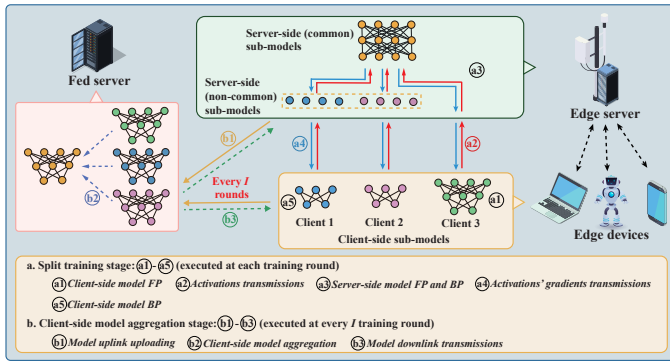


Fig. 1. The illustration of AdaptSFL over edge computing systems.

located on the edge server, should always be synchronized without incurring communication costs¹, which is not the case for aggregating client-side models from distributed edge devices. To demonstrate the impact of client-side MA, Fig. 2 shows that parameter I (client-side sub-models are aggregated every I training rounds) balances the converged accuracy and communication overhead. A smaller I usually leads to higher converged accuracy while incurring more communication costs. On the other hand, concerning the effect of MS, Fig. 3 reveals that a shallow cut layer enhances training accuracy since a larger portion of the model can be synchronized in each training round on the server. However, this may result in increased communication overhead for transmitting cut-layer activations/gradients because a shallower layer in CNNs typically has a larger size of layer output. Overall, optimizing MS and client-side MA requires fundamental tradeoff analysis to accelerate SFL under communication and computing constraints.

This paper aims to minimize the training latency of SFL for achieving target learning performance under resource-constrained edge computing systems. To this end, we propose AdaptSFL, a novel resource-adaptive SFL framework with convergence guarantee, featuring adaptive client-side MA and MS under network resource constraints. To establish the foundation, we first derive a convergence bound of AdaptSFL that characterizes the effect of client-side MA and MS on its training convergence. This derivation is challenging and differs from the analysis of FL because client-side and server-side sub-models should be aggregated at different frequencies in SFL. Following this, we formulate and solve the optimization problem of MS and client-side MA. The main contributions of this paper are summarized as follows:

- We investigate the system optimization for SFL over resource-constrained edge systems. We theoretically analyze the convergence bound of AdaptSFL, providing some intriguing insights that can lay the foundation for SFL optimization. To our best knowledge, this is the first convergence analysis of SFL that characterizes the effect of MS and client-side MA on its training convergence.

¹This is because more frequent model aggregation generally leads to better training convergence as demonstrated by both theoretical analysis and experiments [21].

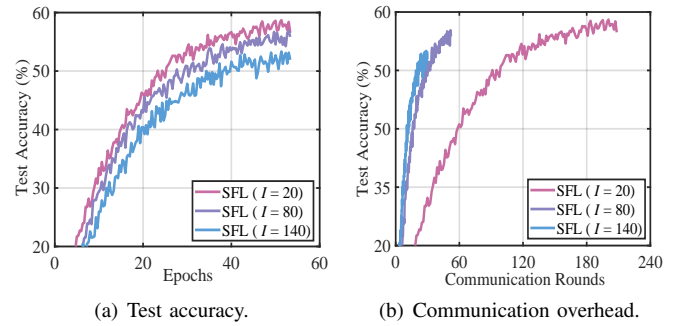


Fig. 2. The impact of client-side MA on training performance and communication overhead. Fig. 2(a) and Fig. 2(b) show the performance for test accuracy versus number of epochs and communication rounds. The experiment is conducted on the CIFAT-10 dataset under the non-IID setting with $L_c = 8$.

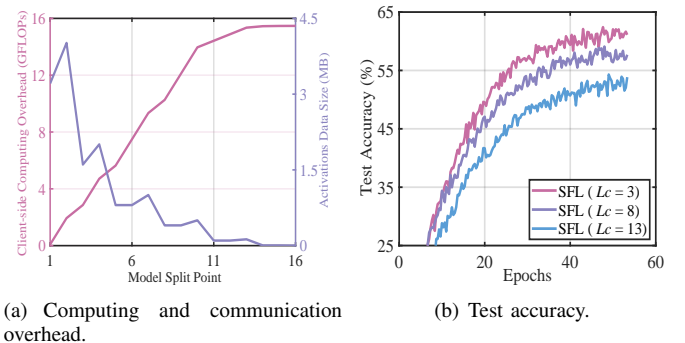


Fig. 3. The impact of MS on computing and communication overhead as well as training performance. Fig. 3(a) shows the computing and communication overhead of SFL at different model split points. Fig. 3(b) presents the performance for test accuracy versus the number of epochs. The experiment is conducted on the CIFAT-10 dataset under the non-IID setting with $I = 15$.

- We leverage the derived convergence bound to formulate a joint optimization problem for client-side MA and MS to minimize the time consumed for model convergence over edge networks.
- We decompose the optimization problem into two tractable subproblems of client-side MA and MS, and develop efficient algorithms to obtain the optimal solutions for them, respectively. Subsequently, we develop an alternating optimization method to obtain an efficient suboptimal solution from the joint problem.
- We conduct extensive simulations across various datasets to validate our theoretical analysis and demonstrate the superiority of the proposed solution over the counterpart without optimization.

The remainder of this paper is organized as follows. Section II introduces related work. Section III elaborates on system model and AdaptSFL framework. Section IV provides the convergence analysis. We formulate the optimization problem in Section V and offer the corresponding solution approach in Section VI. Section VII provides the simulation results. Finally, concluding remarks are presented in Section VIII.

II. RELATED WORK

Tremendous research efforts have been made to improve the learning performance of distributed ML by controlling the model aggregation [13], [21]–[25]. McMahan *et al.* [13] develop a pioneering FedAvg algorithm that enables each participant to conduct multiple local stochastic gradient descent

iterations in a communication round, which aims to reduce the global synchronization frequency without considerably compromising training accuracy. Wang *et al.* [21] propose a control algorithm that determines the best tradeoff between local update and global parameter aggregation to minimize the loss function under a given resource budget. Wu *et al.* [22] devise an adaptive momentum-based FL algorithm to achieve the optimal MA frequency, which lowers the time consumed for achieving the target accuracy. Smith *et al.* [23] and Yu *et al.* [24] empirically design dynamic batch size schemes to reduce MA frequency to establish a more communication-efficient FL framework. Xiang *et al.* [25] propose an adaptive epoch adjustment method to reduce communication rounds by dynamically adjusting MA frequency of end devices. The commonality among these studies lies in convergence analysis, which serves as the basis for optimizing model aggregation. Nevertheless, the aforementioned schemes do not apply to SFL as server-side sub-models, which are co-located at the same place, can always be synchronized in SFL.

MS heavily impacts the training latency of SL, as it leads to varied computing workloads between devices and the server, varied communication overhead due to the diverse output data sizes across layers, and convergence speed owing to the varied proportion of the server-side common model. Several studies have delved into determining the optimal model split point for SL [26]–[28]. Wu *et al.* [26] develop a cluster-based parallel SL framework and a joint cut layer selection, device clustering, and subchannel allocation optimization algorithm to minimize the training overhead considering device heterogeneity and network dynamics. Wang *et al.* [27] present a time-efficient multi-split ML framework, which enables real-time optimal split decisions among multiple computing nodes and dynamically adapts split decisions in response to instantaneous network dynamics. Lin *et al.* [28] propose an efficient parallel SL framework featuring last-layer gradient aggregation, lowering the dimension of activations’ gradients and server-side computing workload. Based on this framework, a joint resource management and MS strategy has been proposed to jointly optimize subchannel allocation, power control, and cut layer selection to minimize the training latency. Unfortunately, these works fail to consider the effect of MS on training convergence.

As can be seen, the problem of optimizing MA and MS to enhance SFL convergence has not been investigated. The problem is non-trivial for two reasons: First, a unified convergence analysis that quantifies the impact of client-side MA and MS on the convergence of SFL is still lacking. Second, considering the heterogeneous bandwidth and computing resources of edge devices, MS and client-side MA need to be jointly optimized to accelerate training convergence, resulting in a complicated optimization problem.

III. RESOURCE-ADAPTIVE SFL FRAMEWORK

In this section, we present the system model in Section III-A and the proposed resource-adaptive SFL framework, named AdaptSFL, in Section III-B.

A. System Model

In this section, we introduce the system model of AdaptSFL to provide a theoretical foundation for the following sections. As illustrated in Fig. 1, we consider a typical scenario of AdaptSFL over edge networks, which consists of three fundamental components:

- **Edge devices:** We consider that each client possesses an edge device with computing capability to execute the client-side forward propagation (FP) and back-propagation (BP). The set of participating edge devices is denoted by $\mathcal{N} = \{1, 2, \dots, N\}$, where N is the number of edge devices. Each edge device i has its local dataset $\mathcal{D}_i = \{\mathbf{x}_{i,k}, y_{i,k}\}_{k=1}^{D_i}$ with D_i data samples, where $\mathbf{x}_{i,k}$ and $y_{i,k}$ are the k -th input data and its corresponding label. The client-side sub-model of edge device i is represented as $\mathbf{w}_{c,i}$.
- **Edge server:** The edge server is a powerful central computing entity responsible for performing server-side sub-model training. The server-side sub-model of edge device i is denoted by $\mathbf{w}_{s,i} = [\mathbf{h}_s; \mathbf{h}_{m,i}]$, where \mathbf{h}_s and $\mathbf{h}_{m,i}$ denote the server-side common and server-side non-common sub-models, respectively. The common sub-model means it is shared by all clients and synchronized in every round. The non-common sub-model stems from the fact that some clients have more layers than others on the server, which is aggregated every I rounds together with the client-side sub-models. Furthermore, the edge server also takes charge of collecting important network information, such as the device computing capabilities and channel states, to support optimization decisions.
- **Fed server:** The fed server takes charge of client-side sub-model synchronization, periodically aggregating the client-side sub-models from all participating edge devices. For privacy concerns, fed and edge servers usually do not belong to the identical party because a malicious server can recover the raw data if getting both client-side sub-models and smashed data [29].

The global model is denoted by $\mathbf{w} = [\mathbf{w}_{s,i}; \mathbf{w}_{c,i}]$. The objective of SL is to find the optimal global model \mathbf{w}^* that achieves good performance across all participating devices, which can be formulated as minimizing a finite-sum non-convex global loss function:

$$\min_{\mathbf{w}} f(\mathbf{w}) \triangleq \min_{\mathbf{w}} \frac{1}{N} \sum_{i=1}^N f_i(\mathbf{w}), \quad (1)$$

where $f_i(\mathbf{w})$ represents the local loss function of edge device i over local dataset \mathcal{D}_i , i.e., $f_i(\mathbf{w}) \triangleq \mathbb{E}_{\xi_i \sim \mathcal{D}_i} [F_i(\mathbf{w}; \xi_i)]$, and ξ_i is training randomness from local dataset \mathcal{D}_i , i.e., stochasticity of data order during training caused by the sampling of mini-batch data. We consider uniformity in the sizes of local datasets across all edge devices for concise expression. Following the standard stochastic optimization setting [30]–[32], it is assumed that the stochastic gradient is an unbiased estimator of the true gradient, i.e., $\mathbb{E}_{\xi_i \sim \mathcal{D}_i} [\nabla F_i(\mathbf{w}_i^{t-1}; \xi_i^t) | \xi_i^{[t-1]}] = \nabla f_i(\mathbf{w}_i^{t-1})$, where $\xi_i^{[t-1]} \triangleq [\xi_i^\tau]_{i \in \{1, 2, \dots, N\}, \tau \in \{1, \dots, t-1\}}$ denotes all the randomness up to training round $t - 1$.

TABLE I
SUMMARY OF IMPORTANT NOTATIONS.

Notation	Description
\mathcal{N}	The set of participating edge devices
\mathcal{D}_i	The local dataset of edge device i
$f(\mathbf{w})$	The global loss function with parameter \mathbf{w}
\mathcal{R}	The set of training rounds
\mathcal{B}_i	The mini-batch drawn from edge device i 's local dataset
b	The mini-batch size
$\mathbf{w}_{c,i}/\mathbf{w}_{s,i}$	The client-side/server-side sub-model of edge device i
\mathbf{h}_s	The server-side common sub-model
$\mathbf{h}_{m,i}$	The server-side non-common sub-model of edge device i
$\mathbf{h}_{c,i}$	The forged client-specific model of edge device i
L_c	The maximum number of layers of client-side sub-models
L	The total number of global model layers
f_s/f_i	The computing capability of server/edge device i
ρ_j/ϖ_j	The FP/BP computing workload of propagating the first j layer neural network for one data sample
ψ_j/χ_j	The data size of the activations/activations' gradients at the cut layer j
δ_j	The data size of client-side sub-model with the cut layer j
$r_i^U/r_{i,f}^U$	The uplink transmission rate from edge device i to edge server/fed server.
$r_i^D/r_{i,f}^D$	The downlink transmission rate from edge server/fed server to edge device i .
$r_{s,f}$	The transmission rate from the edge server to fed server.
$r_{f,s}$	The transmission rate from fed server to edge server.
β, σ_j^2, G_j^2	The loss function constants (detailed in Section IV)
$I, \mu_{i,j}$	The decision variables (explained in Section V)
T_1-T_6	The auxiliary variables (to linearize problem (28))

To solve problem (1), the conventional SFL framework aggregates both client-side and server-side sub-models every training round. However, aggregating client-side sub-models at each training round leads to communication inefficiency, consuming considerable communication resources, especially for implementing SFL over mobile edge devices. Moreover, the MS has not been studied by jointly considering its impact on training convergence and communication-computing workload. Motivated by this, we propose a state-of-the-art AdaptSFL framework capable of resource-adaptive client-side MA and MS. For readers' convenience, the important notations in this paper are summarized in Table 1.

B. The AdaptSFL Framework

This section details the workflow of the proposed AdaptSFL framework. The distinctive feature of AdaptSFL lies in resource-adaptive client-side MA and MS. By optimizing the client-side MA and MS, training latency can be significantly reduced for achieving target learning performance.

Before model training begins, the edge server initializes the ML model, partitions it into client-side and server-side sub-models via layer-wise MS (shown in Section VI), and determines the optimal client-side MA (discussed in Section VI). Afterward, AdaptSFL is executed in I consecutive training rounds. This process loops until the model converges. The training process of AdaptSFL involves two primary stages, i.e., split training and client-side MA. The split training is performed in each training round, while the client-side MA

occurs every I training round. As depicted in Fig. 1, for a training round $t \in \mathcal{R} = \{1, 2, \dots, R\}$, the training process of AdaptSFL is detailed as follows.

a. Split Training Stage: The split training stage involves model updates for participating edge devices and an edge server every training round. This stage comprises the following five steps.

a1) Client-side Model Forward Propagation: In this step, all participating edge devices execute client-side FP in parallel. To be specific, edge device i randomly draws a mini-batch $\mathcal{B}_i \subseteq \mathcal{D}_i$ with b data samples from its local dataset for model training. The input data and corresponding label of mini-batch in training round t are denoted by \mathbf{x}_i^t and \mathbf{y}_i^t , and $\mathbf{w}_{c,i}^{t-1}$ represents the client-side sub-model of edge device i . After feeding a mini-batch of data into the client-side sub-model, activations are generated at the cut layer. The activations of edge device i are represented as

$$\mathbf{a}_i^t = \varphi(\mathbf{x}_i^t; \mathbf{w}_{c,i}^{t-1}), \quad (2)$$

where $\varphi(x; w)$ maps the relationship between input data x and its predicted value given model parameter w .

a2) Activations Transmissions: After completing client-side FP, each edge device sends its respective activations and labels to the edge server (usually over wireless channels). The collected activations from participating edge devices are then utilized to fuel server-side model training.

a3) Server-side Model Forward Propagation and Back-propagation: After receiving activations from participating edge devices, the edge server feeds these activations into the server-side sub-models to execute the server-side FP. For edge device i , the predicted value is expressed as

$$\hat{\mathbf{y}}_i^t = \varphi(\mathbf{a}_i^t; \mathbf{w}_{s,i}^{t-1}), \quad (3)$$

where $\mathbf{w}_{s,i}^{t-1} = [\mathbf{h}_s^{t-1}; \mathbf{h}_{m,i}^{t-1}]$, \mathbf{h}_s^{t-1} and $\mathbf{h}_{m,i}^{t-1}$ denote the server-side common and server-side non-common sub-models, respectively. The predicted value and labels are utilized to calculate loss function value and further derive the server-side sub-model's gradients.

For the server-side common sub-model, the server updates \mathbf{h}_s^t based on

$$\mathbf{h}_s^t = \frac{1}{N} \sum_{i=1}^N \mathbf{h}_{s,i}^t, \quad (4)$$

where $\mathbf{h}_{s,i}^t \leftarrow \mathbf{h}_{s,i}^{t-1} - \gamma \nabla_{\mathbf{h}_s} F_i(\mathbf{h}_{s,i}^{t-1}; \xi_i^t)$ is server-side common sub-model for edge device i and $\nabla_{\mathbf{w}} F(\mathbf{w}; \xi)$ represents the gradient of the function $F(\mathbf{w}; \xi)$ with respect to the model parameter \mathbf{w} . Since the aggregation in Eqn. (4) does not incur any communication overhead, we assume it is conducted every training round to improve training convergence. In this way, the server-side common sub-model is equivalent to centralized training (i.e., stochastic gradient descent or SGD).

Due to the heterogeneous cut layers, some edge devices can leave more layers on the server side, resulting in server-side non-common parts of server-side sub-models. Each edge

²The edge server can execute model update for multiple edge devices in either a serial or parallel fashion, which does not affect training performance. Here, we consider the parallel fashion.

device updates its respective server-side non-common sub-model individually, i.e.,

$$\mathbf{h}_{m,i}^t \leftarrow \mathbf{h}_{m,i}^{t-1} - \gamma \nabla_{\mathbf{h}_m} F_i(\mathbf{h}_{m,i}^{t-1}; \xi_i^t), \quad (5)$$

where $\nabla_{\mathbf{h}_s} F_i(\mathbf{h}_s^{t-1}; \xi_i^t)$ and $\nabla_{\mathbf{h}_m} F_i(\mathbf{h}_{m,i}^{t-1}; \xi_i^t)$ represent the stochastic gradients of server-side common and non-common sub-models of edge device i , and γ is the learning rate.

a4) *Activations' Gradients Transmissions*: After the server-side BP is completed, the edge server transmits the activations' gradients to its corresponding edge devices.

a5) *Client-side Model Back-propagation*: In this step, each edge device updates its client-side sub-model parameters based on the received activations' gradients. For edge device i , the client-side sub-model is updated through

$$\mathbf{w}_{c,i}^t \leftarrow \mathbf{w}_{c,i}^{t-1} - \gamma \nabla_{\mathbf{w}_c} F_i(\mathbf{w}_{c,i}^{t-1}; \xi_i^t). \quad (6)$$

b. *Client-side Model Aggregation Stage*: The client-side MA stage primarily focuses on aggregating forged client-specific sub-models (including client-side sub-models and server-side non-common sub-models specific to each client) on the fed server, which is executed every I training round. This stage consists of the following three steps.

b1) *Model Uplink Uploading*: In this step, edge devices and edge server simultaneously send the client-side sub-models and server-side non-common sub-models to the fed server over the wireless/wired links.

b2) *Client-side Model Aggregation*: The fed server pairs and assembles the received client-side sub-models and server-side non-common sub-models to forge the client-specific models. Afterwards, these forged client-specific models are aggregated, denoted by

$$\mathbf{h}_c^t = \frac{1}{N} \sum_{i=1}^N \mathbf{h}_{c,i}^t, \quad (7)$$

where $\mathbf{h}_{c,i}^t = [\mathbf{h}_{m,i}^t; \mathbf{w}_{c,i}^t]$ is forged client-specific model of edge device i .

b3) *Model Downlink Transmissions*: After completing the client-side MA, the fed server sends updated client-side sub-models and server-side non-common sub-models to corresponding edge devices and the edge server, respectively.

The AdaptSFL training framework is outlined in **Algorithm 1**, where E is the total number of stochastic gradients involved in model training.

IV. CONVERGENCE ANALYSIS FOR THE ADAPTSFL FRAMEWORK

In this section, we provide the first convergence analysis of SFL that characterizes the effect of both client-side MA and MS on its training convergence, which serves as the basis for developing an efficient iterative method in Section VI.

Before analysis, we first clarify several notations to simplify the derivation process and results. Considering the variance in MA frequency, we define the global model of edge device i as $\mathbf{w}_i^t = [\mathbf{h}_{s,i}^t; \mathbf{h}_{c,i}^t]$, which contains server-side common sub-model and forged client-specific model. The server-side common sub-models are aggregated each training round, while the client-specific model is aggregated every I training round.

Algorithm 1 The AdaptSFL Training Framework

Input: $b, \gamma, E, \mathcal{N}$ and \mathcal{D} .

Output: \mathbf{w}^* .

```

1: Initialization:  $\mathbf{w}^0, \mathbf{w}_i^0 \leftarrow \mathbf{w}^0, I^0 \leftarrow 1, \tau \leftarrow 0$  and  $\rho \leftarrow 0$ .
2: while  $b \sum_{\eta=0}^{\tau} I^\eta \leq E$  do
3:   Determine  $I^\tau$  and  $\mu^\tau$  based on Algorithm 3
4:   for  $t = \rho + 1, \rho + 2, \dots, \rho + I^\tau$  do
5:     /** Runs on edge devices **/
6:     for all edge device  $i \in \mathcal{N}$  in parallel do
7:        $\mathbf{a}_i^t \leftarrow \varphi(\mathbf{x}_i^t; \mathbf{w}_{c,i}^{t-1})$ 
8:       Send  $(\mathbf{a}_i^t, \mathbf{y}_i^t)$  to the edge server
9:     end for
10:    end for
11:    /** Runs on edge server **/
12:     $\hat{\mathbf{y}}_i^t = \varphi(\mathbf{a}_i^t; \mathbf{w}_{s,i}^{t-1})$ 
13:    Calculate loss function value  $f(\mathbf{w}^{t-1})$ 
14:     $\mathbf{h}_s^t \leftarrow \mathbf{h}_s^{t-1} - \gamma \frac{1}{N} \sum_{i=1}^N \nabla_{\mathbf{h}_s} F_i(\mathbf{h}_s^{t-1}; \xi_i^t)$ ,
15:     $\mathbf{h}_{m,i}^t \leftarrow \mathbf{h}_{m,i}^{t-1} - \gamma \nabla_{\mathbf{h}_m} F_i(\mathbf{h}_{m,i}^{t-1}; \xi_i^t)$ 
16:    Send activations' gradients to corresponding edge devices
17:    /** Runs on edge devices **/
18:    for all edge device  $i \in \mathcal{N}$  in parallel do
19:       $\mathbf{w}_{c,i}^t \leftarrow \mathbf{w}_{c,i}^{t-1} - \gamma \nabla_{\mathbf{w}_c} F_i(\mathbf{w}_{c,i}^{t-1}; \xi_i^t)$ 
20:    end for
21:    /** Runs on the fed server **/
22:    if  $(t - \rho) \bmod I^\tau = 0$  then
23:      Forge client-side sub-models  $\mathbf{h}_{c,i}^t = [\mathbf{h}_{m,i}^t; \mathbf{w}_{c,i}^t]$ 
24:       $\mathbf{h}_c^t = \frac{1}{N} \sum_{i=1}^N \mathbf{h}_{c,i}^t$ 
25:       $\mathbf{h}_{c,i}^t \leftarrow \mathbf{h}_c^t$ 
26:    end if
27:    end for
28:    Update  $\rho \leftarrow \rho + I^\tau$ 
29:    Update  $\tau \leftarrow \tau + 1$ 
30:  end while

```

The model split point between these two sub-models is L_c , defined as the maximum number of layers of client-side sub-models due to discrepancies in model split points among different edge devices. The corresponding gradients of these two sub-models are determined as

$$\mathbf{g}_{c,i}^t = [\nabla_{\mathbf{h}_m} F_i(\mathbf{h}_{m,i}^{t-1}; \xi_i^t); \nabla_{\mathbf{w}_c} F_i(\mathbf{w}_{c,i}^{t-1}; \xi_i^t)] \quad (8)$$

and

$$\mathbf{g}_{s,i}^t = \sum_{i=1}^N \nabla_{\mathbf{h}_s} F_i(\mathbf{h}_s^{t-1}; \xi_i^t), \quad (9)$$

where $\mathbf{h}_s^t = \frac{1}{N} \sum_{i=1}^N \mathbf{h}_{s,i}^t$. Therefore, the gradient of the global model is represented as $\mathbf{g}_i^t = [\mathbf{g}_{s,i}^t; \mathbf{g}_{c,i}^t]$.

In line with the seminal works in distributed stochastic optimization [33]–[36] where convergence analysis is conducted on an aggregated version of individual solutions, this paper focuses on the convergence analysis of $\mathbf{w}^t = \frac{1}{N} \sum_{i=1}^N \mathbf{w}_i^t$. To analyze the convergence rate of **Algorithm 1**, we consider the following two standard assumptions on the loss functions.

Assumption 1 (Smoothness). *Each local loss function $f_i(\mathbf{w})$ is differentiable and β -smooth, i.e., for any \mathbf{w} and \mathbf{w}' , we have*

$$\|\nabla_{\mathbf{w}} f_i(\mathbf{w}) - \nabla_{\mathbf{w}} f_i(\mathbf{w}')\| \leq \beta \|\mathbf{w} - \mathbf{w}'\|, \forall i. \quad (10)$$

Assumption 2 (Bounded variances and second moments). *The variance and second moments of stochastic gradients for each layer have upper bound:*

$$\mathbb{E}_{\xi_i \sim \mathcal{D}_i} \|\nabla_{\mathbf{w}} F_i(\mathbf{w}; \xi_i) - \nabla_{\mathbf{w}} f_i(\mathbf{w})\|^2 \leq \sum_{j=1}^l \sigma_j^2, \forall \mathbf{w}, \forall i. \quad (11)$$

$$\mathbb{E}_{\xi_i \sim \mathcal{D}_i} \|\nabla_{\mathbf{w}} F_i(\mathbf{w}; \xi_i)\|^2 \leq \sum_{j=1}^l G_j^2, \forall \mathbf{w}, \forall i, \quad (12)$$

where l is number of layers for model \mathbf{w} , σ_j^2 and G_j^2 denote the bounded variance and second order moments for the j -th layer of model \mathbf{w} .

Lemma 1. *Under Assumption 1, Algorithm 1 ensures*

$$\mathbb{E}[\|\mathbf{h}_c^t - \mathbf{h}_{c,i}^t\|^2] \leq 4\gamma^2 I^2 \sum_{j=1}^{L_c} G_j^2, \forall i, \forall t,$$

where I denotes client-side model aggregation frequency and \mathbf{h}_c^t is defined in Eqn. (7).

Proof. See Appendix A. \square

Theorem 1. *Under Assumption 1 and Assumption 2, if $0 < \gamma \leq \frac{1}{\beta}$ in Algorithm 1, then for all $R \geq 1$, we have*

$$\frac{1}{R} \sum_{t=1}^R \mathbb{E}[\|\nabla_{\mathbf{w}} f(\mathbf{w}^{t-1})\|^2] \leq \frac{2\vartheta}{\gamma R} + \frac{\beta\gamma \sum_{j=1}^L \sigma_j^2}{N} + 4\beta^2 \gamma^2 I^2 \sum_{j=1}^{L_c} G_j^2, \quad (13)$$

where $\vartheta = f(\mathbf{w}^0) - f^*$, L and f^* represent the total number of global model layers and minimum value of problem (1).

Proof. See Appendix B. \square

Substituting Eqn. (13) into Eqn. (14) yields **Corollary 1**, revealing a lower bound on the number of training rounds for achieving target convergence accuracy.

Corollary 1. *The number of training rounds R for achieving target convergence accuracy ε , i.e., satisfying*

$$\frac{1}{R} \sum_{t=1}^R \mathbb{E}[\|\nabla_{\mathbf{w}} f(\mathbf{w}^{t-1})\|^2] \leq \varepsilon, \quad (14)$$

is given by

$$R \geq \frac{2\vartheta}{\gamma \left(\varepsilon - \frac{\beta\gamma \sum_{j=1}^L \sigma_j^2}{N} - 4\beta^2 \gamma^2 I^2 \sum_{j=1}^{L_c} G_j^2 \right)}. \quad (15)$$

Insights: Eqn. (15) shows that the number of training rounds for achieving target convergence accuracy ε decreases as I decreases and the cut layer becomes shallow, indicating a faster model convergence rate. Similarly, for a given training round R , more frequent client-side MA and a shallower cut layer result in higher converged accuracy (i.e., smaller ε). These observations align with the experimental results illustrated in Fig. 2 and Fig. 3. However, the improved training performance comes at the cost of increasing communication overhead, leading to longer latency per training round. Therefore, it is essential to optimize MS and client-side MA to accelerate SFL under communication and computing constraints.

V. PROBLEM FORMULATION

The convergence analysis results quantify the impact of client-side MA and MS on model convergence and communication efficiency. In this section, guided by the convergence bounds in Section IV, we formulate a joint client-side MA and MS optimization problem. The objective is to minimize the training latency of AdaptSFL over edge networks with heterogeneous participating devices. Subsequently, we propose a resource-adaptive client-side MA and MS strategy in Section VI. For clarity, the decision variables and definitions are listed below.

- I : $I \in \mathbb{N}^+$ denotes the client-side MA decision variable, which indicates that the forged client-side sub-model is aggregated every I training rounds.
- $\boldsymbol{\mu}$: $\mu_{i,j} \in \{0, 1\}$ is the MS decision variable, where $\mu_{i,j} = 1$ indicates that the j -th neural network layer is selected as the cut layer for edge device i , and 0 otherwise. $\boldsymbol{\mu} = [\mu_{1,1}, \mu_{1,2}, \dots, \mu_{N,L}]$ represents the collection of MS decisions.

A. Training Latency Analysis

In this section, we provide the training latency analysis for each step of AdaptSFL. Without loss of generality, we focus on one training round for analysis. The training round number index t is omitted for notational simplicity. To begin, we analyze the latency of split training stage for one training round as follows.

a1) Client-side Model Forward Propagation Latency: In this step, each edge device utilizes its local dataset to conduct the client-side FP. The computing workload (in FLOPs) of the client-side FP for edge device i per data sample is denoted by $\Phi_{c,i}^F(\boldsymbol{\mu}) = \sum_{j=1}^L \mu_{i,j} \rho_j$, where ρ_j is the FP computing workload of propagating the first j layer of neural network for one data sample. Considering that each edge device randomly draws a mini-batch containing b data samples for executing the client-

side FP, the client-side FP latency of edge device i is calculated as

$$T_i^F = \frac{b \Phi_{c,i}^F(\boldsymbol{\mu})}{f_i}, \forall i \in \mathcal{N}, \quad (16)$$

where f_i denotes the computing capability of edge device i , i.e., the number of float-point operations per second (FLOPS).

a2) Activations Transmissions Latency: After completing the client-side FP, each edge device sends the activations generated at the cut layer to the edge server. Let $\Gamma_{a,i}(\boldsymbol{\mu}) = \sum_{j=1}^L \mu_{i,j} \psi_j$ represent the data size (in bits) of activations for edge device i , where ψ_j denotes the data size of activations at the cut layer j . Since each edge device employs a mini-batch with b data samples, the activations transmissions latency of edge device i is determined as

$$T_{a,i}^U = \frac{b \Gamma_{a,i}(\boldsymbol{\mu})}{r_i^U}, \forall i \in \mathcal{N}. \quad (17)$$

where r_i^U is uplink transmission rate from edge device i to the edge server.

a3) Server-side Model Forward Propagation and Back-propagation Latency: This step involves executing the server-side FP and BP with collected activations from all participating edge devices. Let $\Phi_s^F(\boldsymbol{\mu}) = \sum_{i=1}^N \sum_{j=1}^L \mu_{i,j} (\rho_L - \rho_j)$ represent the computing workload of the server-side FP for each data sample. Similarly, the computing workload of the server-side BP per data sample is denoted by $\Phi_s^B(\boldsymbol{\mu}) = \sum_{i=1}^N \sum_{j=1}^L \mu_{i,j} (\varpi_L - \varpi_j)$, where ϖ_j is the BP computing workload of propagating the first j layer of neural network for one data sample. Consequently, the server-side model FP and BP latency can be obtained from

$$T_s^F = \frac{b \Phi_s^F(\boldsymbol{\mu})}{f_s} \quad (18)$$

and

$$T_s^B = \frac{b \Phi_s^B(\boldsymbol{\mu})}{f_s}, \quad (19)$$

where f_s denotes the computing capability of the edge server.

a4) Activations' Gradients Transmissions Latency: After the server-side BP is completed, the edge server sends the activations' gradients to the corresponding edge devices. Let $\Gamma_{g,i}(\boldsymbol{\mu}) = \sum_{j=1}^L \mu_{i,j} \chi_j$ represent the data size of activations' gradients for edge device i , where χ_j denotes the data size of activations' gradients at the cut layer j . Therefore, the activations' gradients transmissions latency of edge device i is expressed as

$$T_{g,i}^D = \frac{b \Gamma_{g,i}(\boldsymbol{\mu})}{r_i^D}, \forall i \in \mathcal{N}. \quad (20)$$

where r_i^D is downlink transmission rate from edge server to edge device i .

a5) Client-side Model Back-propagation Latency: In this step, each edge device executes client-side BP according to

the received activations' gradients. Let $\Phi_{c,i}^B(\boldsymbol{\mu}) = \sum_{j=1}^L \mu_{i,j} \varpi_j$ denote the computing workload of the client-side BP for edge device i per data sample. As a result, the client-side BP latency of edge device i can be obtained by

$$T_i^B = \frac{b \Phi_{c,i}^B(\boldsymbol{\mu})}{f_i}, \forall i \in \mathcal{N}. \quad (21)$$

Then, we analyze the latency of client-side MA stage every I training round as follows.

b1) Model Uplink Transmissions Latency: In this step, each edge device transmits its client-side sub-model to the fed server, while edge server uploads the server-side non-common sub-models to the fed server for client-side MA. Let $\Lambda_{c,i}(\boldsymbol{\mu}) = \sum_{j=1}^L \mu_{i,j} \delta_j$ represent the data size of client-side sub-model for edge device i , where δ_j is the data size of client-side sub-model with the cut layer j . The total data size of the exchanged server-side non-common sub-models is denoted by

$\Lambda_s(\boldsymbol{\mu}) = N \max_i \left\{ \sum_{j=1}^L \mu_{i,j} \delta_j \right\} - \sum_{i=1}^N \sum_{j=1}^L \mu_{i,j} \delta_j$. Therefore, the uplink transmissions latency for the client-side sub-model and server-side non-common sub-models are expressed as

$$T_{c,i}^U = \frac{\Lambda_{c,i}(\boldsymbol{\mu})}{r_{i,f}^U}, \forall i \in \mathcal{N} \quad (22)$$

and

$$T_s^U = \frac{\Lambda_s(\boldsymbol{\mu})}{r_{s,f}}, \quad (23)$$

where $r_{i,f}^U$ and $r_{s,f}$ represent the transmissions rate from edge device i and edge server to the fed server, respectively.

b2) Client-side Model Aggregation: The fed server aggregates the client-side sub-models and server-side non-common sub-models to forge the aggregated client-specific model. For simplicity, the latency for this part is ignored since the aggregation delay is typically much smaller than other steps [37], [38].

b3) Model Downlink Transmissions Latency: After completing client-side MA, the fed server sends the updated client-side sub-model and server-side non-common sub-model to the corresponding edge devices and edge server. Similarly, the downlink transmission latency for the client-side sub-model and server-side non-common sub-models are calculated by

$$T_{c,i}^D = \frac{\Lambda_{c,i}(\boldsymbol{\mu})}{r_{i,f}^D}, \forall i \in \mathcal{N} \quad (24)$$

and

$$T_s^D = \frac{\Lambda_s(\boldsymbol{\mu})}{r_{f,s}}, \quad (25)$$

where $r_{i,f}^D$ and $r_{f,s}$ denote the transmission rate from the fed server to edge device i and edge server, respectively.

B. Joint Client-side Model Aggregation and Model Splitting Problem Formulation

This section presents the problem formulation of client-side MA and MS with the objective of minimizing the time consumed for model convergence over edge networks. As

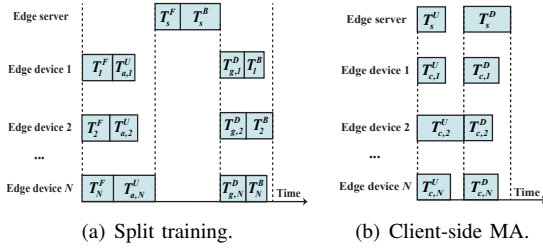


Fig. 4. An illustration of split training and client-side MA stages.

illustrated in Fig. 4, considering that split training is executed per training round and client-side MA occurs every I training round, the total training latency for I training rounds can be derived as

$$T(I, \boldsymbol{\mu}) = I \left\{ \max_i \{T_i^F + T_{a,i}^U\} + T_s^F + T_s^B + \max_i \{T_{g,i}^D + T_i^B\} \right. \\ \left. + \max_i \{T_{c,i}^U, T_s^U\} + \max_i \{T_{c,i}^D, T_s^D\} \right\}. \quad (26)$$

Recalling the derived convergence bound in (13), client-side MA frequency balances the tradeoffs between communication overhead and training convergence, while MS significantly impacts communication-computing overhead, as well as model convergence. Hence, jointly optimizing the client-side MA frequency and MS is imperative to expedite the training process. Observing these facts, we formulate the following optimization problem to minimize the time consumed for model convergence:

$$\begin{aligned} \mathcal{P} : \min_{I, \boldsymbol{\mu}} MT(I, \boldsymbol{\mu}) \quad (27) \\ \text{s.t. C1: } \frac{1}{R} \sum_{t=1}^R \mathbb{E}[\|\nabla_{\mathbf{w}} f(\mathbf{w}^{t-1})\|^2] \leq \varepsilon, \\ \text{C2: } \mu_{i,j} \in \{0, 1\}, \quad \forall i \in \mathcal{N}, j = 1, 2, \dots, L, \\ \text{C3: } \sum_{j=1}^L \mu_{i,j} = 1, \quad \forall i \in \mathcal{N}, \\ \text{C4: } I \in \mathbb{N}^+. \end{aligned}$$

where $M = \frac{R}{T}$ denotes the number of communication rounds for achieving model convergence. Constraint C1 guarantees global convergence accuracy; C2 and C3 ensure that each edge device has a single cut layer, so that the global model is partitioned into client-side and server-side sub-models; C4 denotes that the client-side MA decision variable is a positive integer.

Problem (27) is a combinatorial problem with a non-convex mixed-integer non-linear objective function, which is NP-hard in general. In this case, achieving an optimal solution via polynomial-time algorithms is infeasible.

VI. SOLUTION APPROACH

In this section, we present an efficient iterative algorithm by decoupling the problem (27) into MA and MS subproblems. For each subproblem, the optimal solution can be obtained. We first utilize **Corollary 1** to explicitly express M . It is clear that M is proportional to the objective function, and thus the objective function is minimized if and only if inequality (15)

holds as an equality. Thus, the original problem (27) can be converted into

$$\begin{aligned} \mathcal{P}' : \min_{I, \boldsymbol{\mu}} \Theta(I, \boldsymbol{\mu}) \quad (28) \\ \text{s.t. C2} - \text{C4}, \end{aligned}$$

where

$$\Theta(I, \boldsymbol{\mu}) = \frac{2\vartheta}{\gamma I \left(\varepsilon - \frac{\beta\gamma \sum_{j=1}^L \sigma_j^2}{N} - 4\beta^2\gamma^2 I^2 \sum_{j=1}^{L_c} G_j^2 \right)} T(I, \boldsymbol{\mu}).$$

Problem (28) is still a mixed-integer non-linear programming, and the non-convexity of the objective function makes it still intractable. To solve this problem, we introduce a set of constants $\tilde{\mathbf{G}} = [\tilde{G}_1^2, \tilde{G}_2^2, \dots, \tilde{G}_L^2]$, where \tilde{G}_j^2 denotes the cumulative sum of the bounded second order moments for the first j layers of neural network, defined as

$$\tilde{G}_j^2 = \sum_{k=1}^j G_k^2. \quad (29)$$

Therefore, $\sum_{j=1}^{L_c} G_j^2$ in the objective function can be reformulated as $\max_i \left\{ \sum_{j=1}^L \mu_{i,j} \tilde{G}_j^2 \right\}$. Additionally, we introduce a set of auxiliary variables $\mathbf{T} = [T_1, T_2, \dots, T_6]$ to linearize the objective function, i.e., $\max_i \left\{ \sum_{j=1}^L \mu_{i,j} \tilde{G}_j^2 \right\} \leq T_1$, $\max_i \left\{ \sum_{j=1}^L \mu_{i,j} \delta_j \right\} \leq T_2$, $\max_i \{T_i^F + T_{a,i}^U\} \leq T_3$, $\max_i \{T_{g,i}^D + T_i^B\} \leq T_4$, $\max_i \{T_{c,i}^U, T_s^U\} \leq T_5$, and $\max_i \{T_{c,i}^D, T_s^D\} \leq T_6$. Problem (28) can therefore be transformed into

$$\begin{aligned} \mathcal{P}'' : \min_{I, \boldsymbol{\mu}, \mathbf{T}} \Theta'(I, \boldsymbol{\mu}, \mathbf{T}) \quad (30) \\ \text{s.t. C2} - \text{C4}, \end{aligned}$$

$$\text{R1: } \sum_{j=1}^L \mu_{i,j} \tilde{G}_j^2 \leq T_1, \quad \forall i \in \mathcal{N},$$

$$\text{R2: } \sum_{j=1}^L \mu_{i,j} \delta_j \leq T_2, \quad \forall i \in \mathcal{N},$$

$$\text{R3: } \frac{b \sum_{j=1}^L \mu_{i,j} \rho_j}{f_i} + \frac{b \sum_{j=1}^L \mu_{i,j} \psi_j}{r_i^U} \leq T_3, \quad \forall i \in \mathcal{N},$$

$$\text{R4: } \frac{b \sum_{j=1}^L \mu_{i,j} \chi_j}{r_i^D} + \frac{b \sum_{j=1}^L \mu_{i,j} \varpi_j}{f_i} \leq T_4, \quad \forall i \in \mathcal{N},$$

$$\text{R5: } \frac{\sum_{j=1}^L \mu_{i,j} \delta_j}{r_{i,f}^U} \leq T_5, \quad \forall i \in \mathcal{N},$$

$$\text{R6: } \frac{NT_2 - \sum_{i=1}^N \sum_{j=1}^L \mu_{i,j} \delta_j}{r_{s,f}} \leq T_5,$$

Algorithm 2 Dinkelbach Method for Solving Problem (34)

Input: $\lambda^{(0)}$ satisfying $\Upsilon(\lambda^{(0)}, \boldsymbol{\mu}^{(0)}, \mathbf{T}^{(0)}) \geq 0$, $\boldsymbol{\mu}^{(0)}$, $\mathbf{T}^{(0)}$ and ε_d .

Output: $\boldsymbol{\mu}^*$ and λ^* .

- 1: Initialization: $n \leftarrow 1$.
 - 2: **repeat**
 - 3: Solve problem (35) with $\lambda = \lambda^{(n)}$ to obtain $\boldsymbol{\mu}^{(n)}$ and $\mathbf{T}^{(n)}$
 - 4: Calculate $\Upsilon(\lambda^{(n)}, \boldsymbol{\mu}^{(n)}, \mathbf{T}^{(n)})$
 - 5: $\lambda^{(n+1)} \leftarrow \frac{Q(\boldsymbol{\mu}^{(n)}, \mathbf{T}^{(n)})}{P(\boldsymbol{\mu}^{(n)}, \mathbf{T}^{(n)})}$,
 - 6: $n \leftarrow n + 1$
 - 7: **until** $|\Upsilon(\lambda^{(n)}, \boldsymbol{\mu}^{(n)}, \mathbf{T}^{(n)})| \leq \varepsilon_d$
-

$$\text{R7: } \frac{\sum_{j=1}^L \mu_{i,j} \delta_j}{r_{i,f}^D} \leq T_6 \quad \forall i \in \mathcal{N},$$

$$\text{R8: } \frac{NT_2 - \sum_{i=1}^N \sum_{j=1}^L \mu_{i,j} \delta_j}{r_{f,s}} \leq T_6,$$

where

$$\Theta'(I, \boldsymbol{\mu}, \mathbf{T}) = \frac{2\vartheta \{I \{T_3 + T_s^F + T_s^B + T_4\} + T_5 + T_6\}}{\gamma I \left(\varepsilon - \frac{\beta \gamma \sum_{j=1}^L \sigma_j^2}{N} - 4\beta^2 \gamma^2 I^2 T_1 \right)}. \quad (31)$$

From problem (30), we observe that the introduced auxiliary variables are tightly coupled with the original decision variables, which makes it difficult to solve the problem directly. Hence, we decompose the original problem (30) into two less complicated subproblems based on different decision variables and develop efficient algorithms to tackle each subproblem.

We fix the variables $\boldsymbol{\mu}$ and \mathbf{T} to investigate the subproblem involving client-side MA frequency, which is expressed as

$$\mathcal{P}_1 : \min_I \Theta'(I) \quad (32)$$

s.t. C4.

Then, we have the following theorem:

Theorem 2. *The optimal client-side MA frequency is given by*

$$I^* = \begin{cases} 1 & I' \leq 1 \\ \arg \min_{I \in \{I', [I']\}} \Theta'(I) & I' > 1 \end{cases}, \quad (33)$$

where I' with $\Xi(I') = 0$ can be easily obtained by Newton-Raphson method and $\Xi(I)$ is defined in (47).

Proof. See Appendix C. \square

Therefore, we obtain an optimal solution for problem (32).

By fixing the decision variable I , we convert problem (30) into a standard mixed-integer linear fractional programming (MILFP) with respect to $\boldsymbol{\mu}$ and \mathbf{T} , which is given by

$$\mathcal{P}_2 : \min_{\boldsymbol{\mu}, \mathbf{T}} \Theta'(\boldsymbol{\mu}, \mathbf{T}) \quad (34)$$

s.t. C2, C3, R1 – R8.

Algorithm 3 BCD-based Algorithm.

Input: $I^{(0)}$, $\boldsymbol{\mu}^{(0)}$, $\mathbf{T}^{(0)}$ and ε_b .

Output: I^* and $\boldsymbol{\mu}^*$

- 1: Initialization: $\tau \leftarrow 0$.
 - 2: **repeat**
 - 3: $\tau \leftarrow \tau + 1$
 - 4: Update $I^{(\tau)}$ based on **Theorem 2**
 - 5: Update $\boldsymbol{\mu}^{(\tau)}$ and $\mathbf{T}^{(\tau)}$ based on **Algorithm 2**
 - 6: **until** $|\Theta'(I^{(\tau)}, \boldsymbol{\mu}^{(\tau)}, \mathbf{T}^{(\tau)}) - \Theta'(I^{(\tau-1)}, \boldsymbol{\mu}^{(\tau-1)}, \mathbf{T}^{(\tau-1)})| \leq \varepsilon_b$
-

We utilize the Dinkelbach algorithm [39] to efficiently solve problem (34) by reformulating it as mixed-integer linear programming, which achieves the optimal solution [40], [41]. Introducing the fractional parameter λ , we reformulate problem (34) as

$$\mathcal{P}'_2 : \min_{\boldsymbol{\mu}, \mathbf{T}} \Upsilon(\lambda, \boldsymbol{\mu}, \mathbf{T}) = Q(\boldsymbol{\mu}, \mathbf{T}) - \lambda P(\boldsymbol{\mu}, \mathbf{T}) \quad (35)$$

s.t. C2, C3, R1 – R8,

where

$$Q(\boldsymbol{\mu}, \mathbf{T}) = 2\vartheta \left\{ I \left\{ T_3 + T_s^F + T_s^B + T_4 \right\} + T_5 + T_6 \right\},$$

$$P(\boldsymbol{\mu}, \mathbf{T}) = \gamma I \left(\varepsilon - \frac{\beta \gamma \sum_{j=1}^L \sigma_j^2}{N} - 4\beta^2 \gamma^2 I^2 T_1 \right).$$

The Dinkelbach algorithm iteratively solves problem (35), which is described as follows: We first initialize the fractional parameter $\lambda^{(0)}$ such that $\Upsilon(\lambda^{(0)}, \boldsymbol{\mu}^{(0)}, \mathbf{T}^{(0)}) \geq 0$. At each iteration, we obtain the optimal solution by solving problem (35) with $\lambda^{(n)}$. After that, we update the fractional parameter $\lambda^{(n+1)}$. We repeat the iterations until $|\Upsilon(\lambda^{(n)}, \boldsymbol{\mu}^{(n)}, \mathbf{T}^{(n)})| < \varepsilon_d$, where ε_d is the convergence tolerance. The pseudo-code of the Dinkelbach algorithm for solving problem (34) is given in **Algorithm 2**.

As aforementioned, we decompose the original problem (27) into two tractable subproblems \mathcal{P}_1 and \mathcal{P}_2 according to different decision variables and develop efficient algorithms to solve each subproblem optimally. Based on this, we propose an iterative block-coordinate descent (BCD)-based algorithm [42] to solve problem (27), which is shown in **Algorithm 3**. The key parameters required for executing algorithm (e.g., β , G_j^2 and σ_j^2) are estimated following the approach in [21]. It is noted that, given dynamic network and training conditions, **Algorithm 3** can be conducted every I rounds or longer to accelerate SFL under time-varying edge environments, as illustrated in **Algorithm 1**.

VII. PERFORMANCE EVALUATION

This section provides numerical results to evaluate the learning performance of the proposed AdaptSFL framework and the effectiveness of tailored client-side MA and MS strategy.

A. Simulation Setup

We implement AdaptSFL using Python 3.7 and PyTorch 1.9.1., and train it on a ThinkPad P17 Gen1 laptop equipped with an NVIDIA Quadro RTX 3000 GPU, Intel i9-10885H

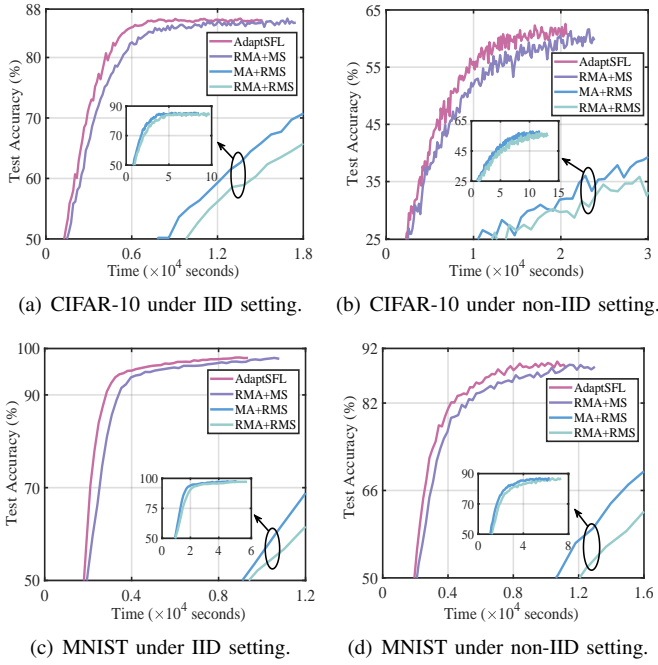


Fig. 5. The training performance for CIFAR-10 and MNIST datasets under IID and non-IID settings using VGG-16.

TABLE II
SIMULATION PARAMETERS.

Parameter	Value	Parameter	Value
f_s	20 TFLOPS	f_i	[1, 2] TFLOPS
N	20	$r_i^U / r_{i,f}^U$	[75, 80] Mbps
$r_i^D / r_{i,f}^D$	370 Mbps	r_s^U / r_s^D	400 Mbps
b	16	γ	5×10^{-4}

CPUs and 4TB SSD. In the simulations, we deploy N edge devices and N is set to 20 by default unless specified otherwise. The computing capability of each edge device is uniformly distributed within [1, 2] TFLOPS, and the computing capability of the server is set to 20 TFLOPS. The uplink transmission rates from edge device i to the edge server and fed server follow uniform distribution within [75, 80] Mbps, and the corresponding downlink rates are set to 370 Mbps. For convenience, the inter-server transmission rate, namely r_s^U and r_s^D , are identically set to 400 Mbps. The mini-batch size and learning rate are set to 16 and 5×10^{-4} . For readers' convenience, the detailed simulation parameters are summarized in Table 2.

We adopt the object detection dataset CIFAR-10 [43] and handwritten digit dataset MNIST [44] to evaluate learning performance of AdaptSFL. The CIFAR-10 dataset contains 10 distinct categories of object images, such as airplanes, automobiles and trucks, and comprises 50000 training samples as well as 10000 test samples. The MNIST dataset includes grayscale images of handwritten digits 0 to 9 with 60000 training samples and 10000 test samples. Furthermore, we conduct experiments under IID and non-IID data settings. The data samples are shuffled and distributed evenly to all edge devices in the IID setting. In the non-IID setting [45]–[47], we sort the data samples by labels, divide them into 40 shards,

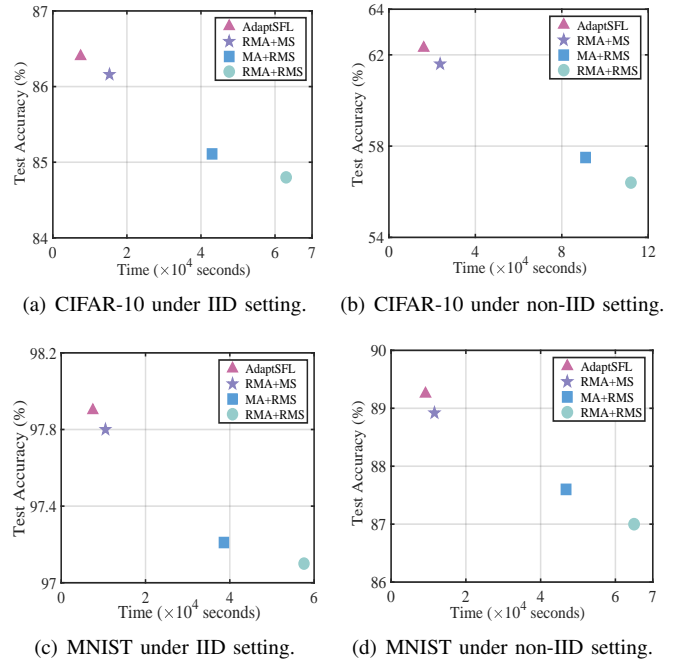


Fig. 6. The converged accuracy and time for CIFAR-10 and MNIST datasets under IID and non-IID settings using VGG-16.

and distribute 2 shards to each of the 20 edge devices.

We deploy the well-known VGG-16 neural network [48]. VGG-16 is a classical deep convolutional neural network comprised of 13 convolution layers and 3 fully connected layers. It leverages the stacking of multiple convolution layers to effectively extract features from images, while the fully connected layers are responsible for classifying and predicting the extracted features.

B. Performance Evaluation of AdaptSFL Framework

In this section, we assess the overall performance of AdaptSFL framework in terms of test accuracy and convergence speed. In addition, we evaluate the robustness of AdaptSFL to varying network resources. To investigate the advantages of AdaptSFL framework, we compare it with three benchmarks:

- **RMA+MS:** The RMA+MS benchmark deploys a random client-side MA strategy (i.e., the client-side MA frequency I is randomly drawn from 1 to 25 during model training.), and employs the adaptive MS scheme in Section VI.
- **MA+RMS:** The MA+RMS benchmark utilizes the adaptive client-side MA strategy in Section VI and adopts a random MS scheme (i.e., randomly selecting model split points during model training).
- **RMA+RMS:** The RMA+RMS benchmark employs the random client-side MA and MS strategy.

Fig. 5 illustrates the training performance of AdaptSFL and three benchmarks on the CIFAR-10 and MNIST datasets. AdaptSFL exhibits faster convergence speed and higher test accuracy compared to the other three benchmarks as the model converges. Notably, AdaptSFL and RMA+MS converge significantly faster than MA+RMS and RMA+RMS owing to the adaptive MS scheme, which strikes a good balance between

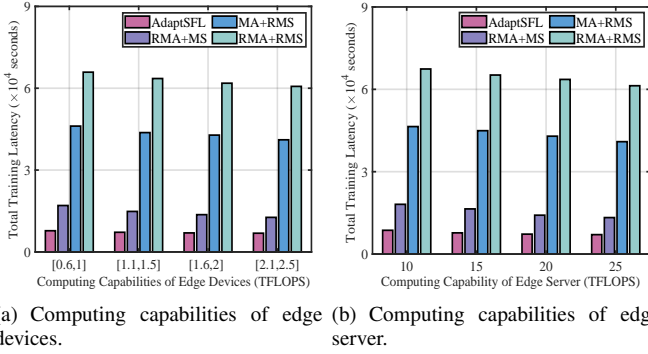


Fig. 7. The converged time versus network computing resources on CIFAR-10 under IID setting.

communication-computing overhead and training convergence speed to expedite model training. Furthermore, the comparison between AdaptSFL and RMA+MS, as well as MA+RMA and RMA+RMS, shows that the tailored client-side MA strategy can further accelerate model training without deteriorating training accuracy. By comparing Fig. 5(a) with Fig. 5(b), and Fig. 5(c) with Fig. 5(d), reveals that the convergence speed of AdaptSFL and other three benchmarks are slower under non-IID setting than under IID setting.

Fig. 6 presents converged accuracy and time (i.e., the incremental increase in test accuracy is lower than 0.02%) for CIFAR-10 and MNIST datasets. Comparing AdaptSFL with RMA+MS and MA+RMS reveals a substantial impact of client-side MA frequency and MS on converged accuracy and time. Moreover, the impact of MS on model training outweighs that of MA frequency. This is because the choice of model split points directly determines the overall aggregation frequency of the global model, e.g., shallower model split points (fewer client-side sub-model layers) imply larger portions of the model are aggregated at each training round. In the IID setting, unoptimized MS leads to 1.5% accuracy degradation and nearly five-fold convergence deceleration on the CIFAR-10 dataset, which is 6.2 and 4.6 times that of unoptimized MA. Furthermore, this difference is more pronounced under the non-IID setting, reaching approximately 7.3 and 10 times, due to model bias caused by discrepancies across local datasets, consistent with FL. The comparison between AdaptSFL and RMA+RMS shows that AdaptSFL achieves a convergence speed improvement of at least 7.7 times over its counterpart without optimization while guaranteeing training accuracy, demonstrating the superior performance of the AdaptSFL framework.

Fig. 7-8 show the converged time versus network computing and communication resources on CIFAR-10 under IID setting. AdaptSFL exhibits significantly shorter converged times than the other three benchmarks across varying computing and communication resources. As network resources decline, the convergence speed of RMA+RMS noticeably slows down. This is because it neither optimizes model split points to strike a balance between computing and communication overheads nor optimizes the client-side MA frequency for expediting model training. The comparison between RMA+MS and MA+RMS reveals that optimizing MA frequency or

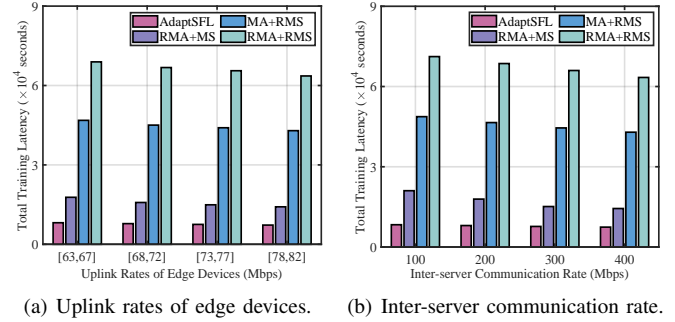


Fig. 8. The converged time versus network communication resources on CIFAR-10 under IID setting.

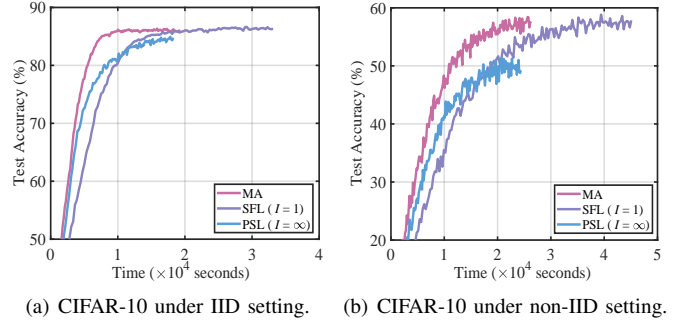


Fig. 9. Ablation experiments for MA strategy on the CIFAR-10 dataset under IID and non-IID setting with $L_c = 8$, where parallel split learning (PSL) [17] is a special case of SFL when $I = \infty$.

MS somewhat mitigates the rise in convergence time with reduced network resources. In contrast, the converged time of AdaptSFL only experiences a slight increase with diminishing network resources, owing to its resource-adaptive client-side MA and MS design. Specifically, as network resources vary, AdaptSFL can optimize MS according to resource conditions and accelerate model convergence by adjusting client-side MA frequency to achieve the minimum communication rounds required for model convergence. This demonstrates the robustness of AdaptSFL to network resources and highlights the adaptability of client-side MA and MS strategies to changes in network resources.

C. Ablation Study of The AdaptSFL Framework

In this section, we conduct ablation experiments to illustrate the effectiveness of each component in AdaptSFL.

Fig. 9 shows the impact of MA frequency on training performance for the CIFAR-10 dataset. PSL [17] exhibits the slowest convergence rate and lowest convergence accuracy due to its lack of client-side MA, leading to inferior generalization performance of local client-side sub-models on the global dataset. In contrast, the proposed resource-adaptive MA strategy expedites model convergence while retaining accuracy comparable to SFL with $I = 1$ (equivalent to centralized learning performance). The proposed client-side MA strategy achieves 1.5% and 5.1% higher convergence accuracy than PSL, and the convergence time is improved by a factor of 1.8 and 1.9 compared to SFL with $I = 1$ under IID and non-IID settings. This improvement stems from its ability to dynamically adjust MA frequency to achieve the minimum communication-computing latency required for

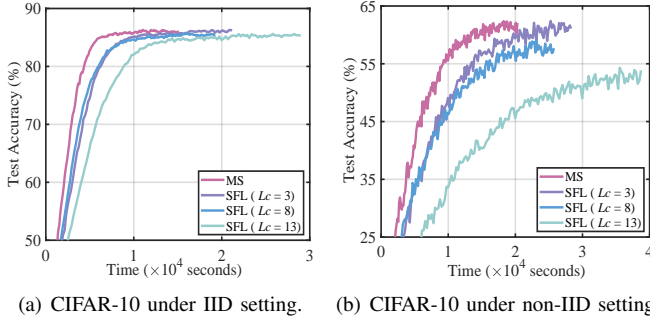


Fig. 10. Ablation experiments for MS scheme on the CIFAR-10 dataset under IID and non-IID setting with $I = 15$.

model convergence. Hence, the effectiveness of the proposed MA scheme is demonstrated.

Fig. 10 presents the impact of MS on training performance for the CIFAR-10 dataset. It can be seen that the convergence accuracy and speed decrease with the deepening of model split point L_c , consistent with the derived convergence boundary in Eqn. (13). This is because deeper model split points result in the smaller portion of global model being aggregated per training round, leading to a lower overall update frequency of the whole model. Furthermore, the impact of MS on convergence accuracy and speed is more significant under non-IID than IID settings. This is attributed to the higher sensitivity of local dataset distribution discrepancies to MA under non-IID setting. The comparisons between MS and the other three benchmarks reveal that the proposed MS strategy can accelerate model convergence while guaranteeing training performance. This demonstrates the superior performance of the tailored MS strategy.

VIII. CONCLUSIONS

In this paper, we propose a SFL framework, named AdaptSFL, to minimize the training latency of SFL over edge networks. We first devise a resource-adaptive client-side MA scheme to achieve the optimal tradeoff between communication overhead and model convergence speed. Then, an optimal MS scheme is designed to determine different model split points based on the resource and data heterogeneity of the clients. To guide the design, we first derive a convergence bound of AdaptSFL, serving as the basis for optimizing the above decision variables. Simulation results demonstrate that our proposed AdaptSFL framework achieves the target accuracy with significantly less time budget compared to benchmarks, demonstrating the effectiveness of the tailored client-side MA and MS strategy.

This work has demonstrated the potential of integrating SFL and edge computing paradigm. However, more research attention needs to be paid to further enhance the time efficiency of SFL. The optimization of other key training hyperparameters, such as batch size and learning rate, is worth further exploration under resource-constrained systems.

APPENDIX

A. PROOF OF LEMMA 1

Fix training round $t \geq 1$. Considering the largest $t_0 \leq t$ that satisfies $t_0 \bmod I = 0$ (Note that such t_0 must exist and $t - t_0 \leq I$.) Recalling the Eqn. (5), Eqn. (6) and Eqn. (8) for updating the model weights, that

$$\mathbf{h}_{c,i}^t = \mathbf{h}_c^{t_0} - \gamma \sum_{\tau=t_0+1}^t \mathbf{g}_{c,i}^\tau \quad (36)$$

By (7), we have

$$\mathbf{h}_c^t = \mathbf{h}_c^{t_0} - \gamma \sum_{\tau=t_0+1}^t \frac{1}{N} \sum_{i=1}^N \mathbf{g}_{c,i}^\tau$$

Thus, we have

$$\begin{aligned} & \mathbb{E}[\|\mathbf{h}_c^t - \mathbf{h}_{c,i}^t\|^2] \\ &= \mathbb{E}[\|\gamma \sum_{\tau=t_0+1}^t \frac{1}{N} \sum_{i=1}^N \mathbf{g}_{c,i}^\tau - \gamma \sum_{\tau=t_0+1}^t \mathbf{g}_{c,i}^\tau\|^2] \\ &= \gamma^2 \mathbb{E}[\|\sum_{\tau=t_0+1}^t \frac{1}{N} \sum_{i=1}^N \mathbf{g}_{c,i}^\tau - \sum_{\tau=t_0+1}^t \mathbf{g}_{c,i}^\tau\|^2] \\ &\stackrel{(a)}{\leq} 2\gamma^2 \mathbb{E}[\|\sum_{\tau=t_0+1}^t \frac{1}{N} \sum_{i=1}^N \mathbf{g}_{c,i}^\tau\|^2 + \|\sum_{\tau=t_0+1}^t \mathbf{g}_{c,i}^\tau\|^2] \\ &\stackrel{(b)}{\leq} 2\gamma^2(t-t_0) \mathbb{E}[\sum_{\tau=t_0+1}^t \|\frac{1}{N} \sum_{i=1}^N \mathbf{g}_{c,i}^\tau\|^2 + \sum_{\tau=t_0+1}^t \|\mathbf{g}_{c,i}^\tau\|^2] \\ &\stackrel{(c)}{\leq} 2\gamma^2(t-t_0) \mathbb{E}[\sum_{\tau=t_0+1}^t (\frac{1}{N} \sum_{i=1}^N \|\mathbf{g}_{c,i}^\tau\|^2) + \sum_{\tau=t_0+1}^t \|\mathbf{g}_{c,i}^\tau\|^2] \\ &\stackrel{(d)}{\leq} 4\gamma^2 I^2 \sum_{j=1}^{L_c} G_j^2 \end{aligned}$$

where (a)-(c) follows by using the inequality $\|\sum_{i=1}^n \mathbf{z}_i\|^2 \leq n \sum_{i=1}^n \|\mathbf{z}_i\|^2$ for any vectors \mathbf{z}_i and any positive integer n (using $n = 2$ in (a), $n = t - t_0$ in (b) and $n = N$ in (c)); and (d) follows from **Assumption 2**.

B. PROOF OF THEOREM 1

For training round $t \geq 1$. By the smoothness of loss function $f(\cdot)$, we have

$$\begin{aligned} \mathbb{E}[f(\mathbf{w}^t)] &\leq \mathbb{E}[f(\mathbf{w}^{t-1})] + \mathbb{E}[\langle \nabla_{\mathbf{w}} f(\mathbf{w}^{t-1}), \mathbf{w}^t - \mathbf{w}^{t-1} \rangle] \\ &\quad + \frac{\beta}{2} \mathbb{E}[\|\mathbf{w}^t - \mathbf{w}^{t-1}\|^2]. \end{aligned} \quad (37)$$

Note that

$$\begin{aligned} & \mathbb{E}[\|\mathbf{w}^t - \mathbf{w}^{t-1}\|^2] \\ &= \mathbb{E}[\|[\mathbf{h}_c^t; \mathbf{h}_s^t] - [\mathbf{h}_c^{t-1}; \mathbf{h}_s^{t-1}]\|^2] \\ &= \mathbb{E}[\|[\mathbf{h}_c^t - \mathbf{h}_c^{t-1}; \mathbf{h}_s^t - \mathbf{h}_s^{t-1}]\|^2] \\ &= \mathbb{E}[\|\mathbf{h}_c^t - \mathbf{h}_c^{t-1}\|^2] + \mathbb{E}[\|\mathbf{h}_s^t - \mathbf{h}_s^{t-1}\|^2], \end{aligned} \quad (38)$$

where $\mathbb{E}[\|\mathbf{h}_c^t - \mathbf{h}_c^{t-1}\|^2]$ can be bounded as

$$\begin{aligned}
 & \mathbb{E}[\|\mathbf{h}_c^t - \mathbf{h}_c^{t-1}\|^2] \stackrel{(a)}{=} \gamma^2 \mathbb{E}[\|\frac{1}{N} \sum_{i=1}^N \mathbf{g}_{c,i}^t\|^2] \\
 & \stackrel{(b)}{=} \gamma^2 \mathbb{E}[\|\frac{1}{N} \sum_{i=1}^N (\mathbf{g}_{c,i}^t - \nabla_{\mathbf{h}_c} f_i(\mathbf{h}_{c,i}^{t-1}))\|^2] \\
 & + \gamma^2 \mathbb{E}[\|\frac{1}{N} \sum_{i=1}^N \nabla_{\mathbf{h}_c} f_i(\mathbf{h}_{c,i}^{t-1})\|^2] \\
 & \stackrel{(c)}{=} \frac{\gamma^2}{N^2} \sum_{i=1}^N \mathbb{E}[\|\mathbf{g}_{c,i}^t - \nabla_{\mathbf{h}_c} f_i(\mathbf{h}_{c,i}^{t-1})\|^2] \\
 & + \gamma^2 \mathbb{E}[\|\frac{1}{N} \sum_{i=1}^N \nabla_{\mathbf{h}_c} f_i(\mathbf{h}_{c,i}^{t-1})\|^2] \\
 & \stackrel{(d)}{\leq} \frac{\gamma^2 \sum_{j=1}^{L_c} \sigma_j^2}{N} + \gamma^2 \mathbb{E}[\|\frac{1}{N} \sum_{i=1}^N \nabla_{\mathbf{h}_c} f_i(\mathbf{h}_{c,i}^{t-1})\|^2]. \quad (39)
 \end{aligned}$$

where (a) follows from Eqn. (7) and Eqn. (36); (b) follows by observing that $\mathbb{E}[\mathbf{g}_{c,i}^t] = \nabla_{\mathbf{h}_c} f_i(\mathbf{h}_{c,i}^{t-1})$ and applying the equality $\mathbb{E}[\|\mathbf{z}\|^2] = \mathbb{E}[\|\mathbf{z} - \mathbb{E}[\mathbf{z}]\|^2] + \|\mathbb{E}[\mathbf{z}]\|^2$ that holds for any random vector \mathbf{z} ; (c) follows because each $\mathbf{g}_{c,i}^t - \nabla_{\mathbf{h}_c} f_i(\mathbf{h}_{c,i}^{t-1})$ has zero mean and is independent across edge devices; and (d) follows from **Assumption 2**.

Similarly, $\mathbb{E}[\|\mathbf{h}_s^t - \mathbf{h}_s^{t-1}\|^2]$ has an upper bound:

$$\mathbb{E}[\|\mathbf{h}_s^t - \mathbf{h}_s^{t-1}\|^2] \leq \frac{\gamma^2 \sum_{j=L_c+1}^L \sigma_j^2}{N} + \gamma^2 \mathbb{E}[\|\frac{1}{N} \sum_{i=1}^N \nabla_{\mathbf{h}_s} f_i(\mathbf{h}_{s,i}^{t-1})\|^2]. \quad (40)$$

Substituting Eqn. (39) and Eqn. (40) into Eqn. (38) yields

$$\begin{aligned}
 & \mathbb{E}[\|\mathbf{w}^t - \mathbf{w}^{t-1}\|^2] \\
 & \leq \frac{\gamma^2 \sum_{j=1}^L \sigma_j^2}{N} + \gamma^2 \mathbb{E}[\|\frac{1}{N} \sum_{i=1}^N \nabla_{\mathbf{h}_c} f_i(\mathbf{h}_{c,i}^{t-1})\|^2] \\
 & + \gamma^2 \mathbb{E}[\|\frac{1}{N} \sum_{i=1}^N \nabla_{\mathbf{h}_s} f_i(\mathbf{h}_{s,i}^{t-1})\|^2] \\
 & = \frac{\gamma^2 \sum_{j=1}^L \sigma_j^2}{N} + \gamma^2 \mathbb{E}[\|\frac{1}{N} \sum_{i=1}^N \nabla_{\mathbf{w}} f_i(\mathbf{w}_i^{t-1})\|^2] \quad (41)
 \end{aligned}$$

We further note that

$$\begin{aligned}
 & \mathbb{E}[\langle \nabla_{\mathbf{w}} f(\mathbf{w}^{t-1}), \mathbf{w}^t - \mathbf{w}^{t-1} \rangle] \\
 & \stackrel{(a)}{=} -\gamma \mathbb{E}[\langle \nabla_{\mathbf{w}} f(\mathbf{w}^{t-1}), \frac{1}{N} \sum_{i=1}^N \mathbf{g}_i^t \rangle] \\
 & \stackrel{(b)}{=} -\gamma \mathbb{E}[\langle \nabla_{\mathbf{w}} f(\mathbf{w}^{t-1}), \frac{1}{N} \sum_{i=1}^N \nabla_{\mathbf{w}} f_i(\mathbf{w}_i^{t-1}) \rangle] \\
 & \stackrel{(c)}{=} -\frac{\gamma}{2} \mathbb{E}[\|\nabla_{\mathbf{w}} f(\mathbf{w}^{t-1})\|^2 + \|\frac{1}{N} \sum_{i=1}^N \nabla_{\mathbf{w}} f_i(\mathbf{w}_i^{t-1})\|^2] \\
 & - \|\nabla_{\mathbf{w}} f(\mathbf{w}^{t-1}) - \frac{1}{N} \sum_{i=1}^N \nabla_{\mathbf{w}} f_i(\mathbf{w}_i^{t-1})\|^2] \quad (42)
 \end{aligned}$$

where (a) follows from $\mathbf{w}^t = \frac{1}{N} \sum_{i=1}^N \mathbf{w}_i^t$; (c) follows from the identity $\langle \mathbf{z}_1, \mathbf{z}_2 \rangle = \frac{1}{2} (\|\mathbf{z}_1\|^2 + \|\mathbf{z}_2\|^2 - \|\mathbf{z}_1 - \mathbf{z}_2\|^2)$ for any two vectors $\mathbf{z}_1, \mathbf{z}_2$ of the same length; (b) follows from

$$\begin{aligned}
 & \mathbb{E}[\langle \nabla_{\mathbf{w}} f(\mathbf{w}^{t-1}), \frac{1}{N} \sum_{i=1}^N \mathbf{g}_i^t \rangle] \\
 & = \mathbb{E}[\mathbb{E}[\langle \nabla_{\mathbf{w}} f(\mathbf{w}^{t-1}), \frac{1}{N} \sum_{i=1}^N \mathbf{g}_i^t \rangle | \boldsymbol{\xi}^{[t-1]}]] \\
 & = \mathbb{E}[\langle \nabla_{\mathbf{w}} f(\mathbf{w}^{t-1}), \frac{1}{N} \sum_{i=1}^N \mathbb{E}[\mathbf{g}_i^t | \boldsymbol{\xi}^{[t-1]}] \rangle] \\
 & = \mathbb{E}[\langle \nabla_{\mathbf{w}} f(\mathbf{w}^{t-1}), \frac{1}{N} \sum_{i=1}^N \nabla_{\mathbf{w}} f_i(\mathbf{w}_i^{t-1}) \rangle]
 \end{aligned}$$

where the first equality follows by the law of expectations, the second equality follows because \mathbf{w}^{t-1} is determined by $\boldsymbol{\xi}^{[t-1]} = [\boldsymbol{\xi}^1, \dots, \boldsymbol{\xi}^{t-1}]$ and the third equality follows from $\mathbb{E}[\mathbf{g}_i^t | \boldsymbol{\xi}^{[t-1]}] = \mathbb{E}[\nabla F_i(\mathbf{w}_i^{t-1}; \boldsymbol{\xi}_i^t) | \boldsymbol{\xi}^{[t-1]}] = \nabla f_i(\mathbf{w}_i^{t-1})$.

Substituting Eqn. (41) and Eqn. (42) into Eqn. (37), we have

$$\begin{aligned}
 & \mathbb{E}[f(\mathbf{w}^t)] \\
 & \leq \mathbb{E}[f(\mathbf{w}^{t-1})] - \frac{\gamma - \gamma^2 \beta}{2} \mathbb{E}[\|\frac{1}{N} \sum_{i=1}^N \nabla_{\mathbf{w}} f_i(\mathbf{w}_i^{t-1})\|^2] \\
 & - \frac{\gamma}{2} \mathbb{E}[\|\nabla_{\mathbf{w}} f(\mathbf{w}^{t-1})\|^2] + \frac{\beta \gamma^2 \sum_{j=1}^L \sigma_j^2}{2N} \\
 & + \frac{\gamma}{2} \mathbb{E}[\|\nabla_{\mathbf{w}} f(\mathbf{w}^{t-1}) - \frac{1}{N} \sum_{i=1}^N \nabla_{\mathbf{w}} f_i(\mathbf{w}_i^{t-1})\|^2] \\
 & \stackrel{(a)}{\leq} \mathbb{E}[f(\mathbf{w}^{t-1})] - \frac{\gamma}{2} \mathbb{E}[\|\nabla_{\mathbf{w}} f(\mathbf{w}^{t-1})\|^2] + \frac{\beta \gamma^2 \sum_{j=1}^L \sigma_j^2}{2N} \\
 & + \frac{\gamma}{2} \mathbb{E}[\|\nabla_{\mathbf{h}_c} f(\mathbf{h}_c^{t-1}) - \frac{1}{N} \sum_{i=1}^N \nabla_{\mathbf{h}_c} f_i(\mathbf{h}_{c,i}^{t-1})\|^2] \\
 & + \frac{\gamma}{2} \mathbb{E}[\|\nabla_{\mathbf{h}_s} f(\mathbf{h}_s^{t-1}) - \frac{1}{N} \sum_{i=1}^N \nabla_{\mathbf{h}_s} f_i(\mathbf{h}_{s,i}^{t-1})\|^2] \\
 & \stackrel{(b)}{\leq} \mathbb{E}[f(\mathbf{w}^{t-1})] - \frac{\gamma}{2} \mathbb{E}[\|\nabla_{\mathbf{w}} f(\mathbf{w}^{t-1})\|^2] + \frac{\beta \gamma^2 \sum_{j=1}^L \sigma_j^2}{2N} \\
 & + 2\beta^2 \gamma^3 I^2 \sum_{j=1}^{L_c} G_j^2 \quad (43)
 \end{aligned}$$

where (a) follows from $0 < \gamma \leq \frac{1}{\beta}$ and (b) holds because of the following inequality (44) and (45)

$$\begin{aligned}
 & \mathbb{E}[\|\nabla_{\mathbf{h}_c} f(\mathbf{h}_c^{t-1}) - \frac{1}{N} \sum_{i=1}^N \nabla_{\mathbf{h}_c} f_i(\mathbf{h}_{c,i}^{t-1})\|^2] \\
 & = \mathbb{E}[\|\frac{1}{N} \sum_{i=1}^N \nabla_{\mathbf{h}_c} f_i(\mathbf{h}_{c,i}^{t-1}) - \frac{1}{N} \sum_{i=1}^N \nabla_{\mathbf{h}_c} f_i(\mathbf{h}_{c,i}^{t-1})\|^2] \\
 & = \frac{1}{N^2} \mathbb{E}[\|\sum_{i=1}^N (\nabla_{\mathbf{h}_c} f_i(\mathbf{h}_{c,i}^{t-1}) - \nabla_{f,c,i}(\mathbf{h}_{c,i}^{t-1}))\|^2]
 \end{aligned}$$

$$\begin{aligned}
 & \leq \frac{1}{N} \mathbb{E} \left[\sum_{i=1}^N \|\nabla_{\mathbf{h}_c} f_i(\mathbf{h}_c^{t-1}) - \nabla_{\mathbf{h}_c} f_i(\mathbf{h}_{c,i}^{t-1})\|^2 \right] \\
 & \leq \beta^2 \frac{1}{N} \sum_{i=1}^N \mathbb{E} [\|\mathbf{h}_c^{t-1} - \mathbf{h}_{c,i}^{t-1}\|^2] \\
 & \leq 4\beta^2 \gamma^2 I^2 \sum_{j=1}^{L_c} G_j^2 \quad (44)
 \end{aligned}$$

where the first inequality follows by using $\|\sum_{i=1}^N \mathbf{z}_i\|^2 \leq N \sum_{i=1}^N \|\mathbf{z}_i\|^2$ for any vectors \mathbf{z}_i ; the second inequality follows from the smoothness of each f_i by **Assumption 1**; and the third inequality follows from **Lemma 1**, and

$$\begin{aligned}
 & \mathbb{E} \left[\|\nabla_{\mathbf{h}_s} f(\mathbf{h}_s^{t-1}) - \frac{1}{N} \sum_{i=1}^N \nabla_{\mathbf{h}_s} f_i(\mathbf{h}_{s,i}^{t-1})\|^2 \right] \\
 & \leq \beta^2 \frac{1}{N} \sum_{i=1}^N \mathbb{E} [\|\mathbf{h}_s^{t-1} - \mathbf{h}_{s,i}^{t-1}\|^2] \stackrel{(a)}{=} 0 \quad (45)
 \end{aligned}$$

where (a) holds because the server-side sub-models are aggregated in each training round (i.e., $I = 1$). Therefore, at any training round t , the server-side sub-model of each edge device is the aggregated version of server-side sub-models.

Dividing Eqn. (43) both sides by $\frac{\gamma}{2}$ and rearranging terms yields

$$\begin{aligned}
 & \mathbb{E} [\|\nabla_{\mathbf{w}} f(\mathbf{w}^{t-1})\|^2] \\
 & \leq \frac{2}{\gamma} (\mathbb{E} [f(\mathbf{w}^{t-1})] - \mathbb{E} [f(\mathbf{w}^t)]) + \frac{\beta\gamma \sum_{j=1}^L \sigma_j^2}{N} + 4\beta^2 \gamma^2 I^2 \sum_{j=1}^{L_c} G_j^2
 \end{aligned}$$

Summing over $t \in \{1, \dots, R\}$ and dividing both sides by R yields

$$\begin{aligned}
 & \frac{1}{R} \sum_{t=1}^R \mathbb{E} [\|\nabla_{\mathbf{w}} f(\mathbf{w}^{t-1})\|^2] \\
 & \leq \frac{2}{\gamma R} (f(\mathbf{w}^0) - \mathbb{E} [f(\mathbf{w}^R)]) + \frac{\beta\gamma \sum_{j=1}^L \sigma_j^2}{N} + 4\beta^2 \gamma^2 I^2 \sum_{j=1}^{L_c} G_j^2 \\
 & \stackrel{(a)}{\leq} \frac{2}{\gamma R} (f(\mathbf{w}^0) - f^*) + \frac{\beta\gamma \sum_{j=1}^L \sigma_j^2}{N} + 4\beta^2 \gamma^2 I^2 \sum_{j=1}^{L_c} G_j^2
 \end{aligned}$$

where (a) follows because f^* is the minimum value of problem (1).

C. PROOF OF THEOREM 2

We first conduct a functional analysis for the objective function in problem (32). Let $\Theta'(I) = \frac{2\vartheta\{aI+b\}}{\gamma I(c-4\beta^2\gamma^2 I^2 T_1)}$, where

$a = T_3 + T_s^F + T_s^B + T_4$, $b = T_5 + T_6$ and $c = \varepsilon - \frac{\beta\gamma \sum_{j=1}^L \sigma_j^2}{N}$. Taking the first-order derivative of $\Theta'(I)$ yields

$$\frac{\partial \Theta'(I)}{\partial I} = \frac{2\vartheta}{\gamma} \frac{\Xi(I)}{(cI - 4\beta^2\gamma^2 I^3 T_1)^2} \quad (46)$$

where

$$\Xi(I) = 8a\beta^2\gamma^2 I^3 T_1 + 12b\beta^2\gamma^2 I^2 T_1 - bc. \quad (47)$$

Since $\frac{\partial \Xi(I)}{\partial I} = 24\beta^2\gamma^2 I T_1 (aI + b) > 0$, $\Xi(I)$ is an increasing function of I . Considering that $\Xi(0) = -bc < 0$ and $\lim_{I \rightarrow +\infty} \Xi(I) = +\infty > 0$, there must exist I' satisfying $\Xi(I') = 0$ for $I' \in (0, +\infty)$, which can be easily obtained by classical Newton-Raphson method. Then, we see that $\frac{\partial \Theta'(I)}{\partial I} \leq 0$ for $I \in (0, I']$ and $\frac{\partial \Theta'(I)}{\partial I} \geq 0$ for $I \in (I', +\infty)$, which means that the objective function decreases and then increases with respect to I and thus reaches a minimum at $I = I'$.

Based on constraint C4 and the characteristics of the objective function analyzed above, it is obvious that the optimal value I^* only exists on both sides of I' , i.e.,

$$I^* = \begin{cases} 1 & I' \leq 1 \\ \arg \min_{I \in \{I', \lceil I' \rceil\}} \Theta'(I) & I' > 1 \end{cases}, \quad (48)$$

where $\lfloor \cdot \rfloor$ and $\lceil \cdot \rceil$ denote floor and ceiling operations.

REFERENCES

- [1] "How You Contribute to Today's Growing DataSphere and Its Enterprise Impact." IDC. Nov. 2019. [Online]. Available: <https://blogs.idc.com/2019/11/04/how-you-contribute-to-todays-growing-data-sphere-and-its-enterprise-impact/>
- [2] K. B. Letaief, Y. Shi, J. Lu, and J. Lu, "Edge Artificial Intelligence for 6G: Vision, Enabling Technologies, and Applications," *IEEE J. Sel. Areas Commun.*, vol. 40, no. 1, pp. 5–36, Jan. 2022.
- [3] G. Zhu, D. Liu, Y. Du, C. You, J. Zhang, and K. Huang, "Toward an Intelligent Edge: Wireless Communication Meets Machine Learning," *IEEE Commun. Mag.*, vol. 58, no. 1, pp. 19–25, Jan. 2020.
- [4] Z. Lin, L. Wang, J. Ding, B. Tan, and S. Jin, "Channel Power Gain Estimation for Terahertz Vehicle-to-infrastructure Networks," *IEEE Commun. Lett.*, vol. 27, no. 1, pp. 155–159, Jan. 2023.
- [5] S. Hu, Z. Fang, Y. Deng, X. Chen, and Y. Fang, "Collaborative Perception for Connected and Autonomous Driving: Challenges, Possible Solutions and Opportunities," *arXiv preprint arXiv:2401.01544*, Jan. 2024.
- [6] Z. Fang, Z. Lin, Z. Chen, X. Chen, Y. Gao, and Y. Fang, "Automated Federated Pipeline for Parameter-Efficient Fine-Tuning of Large Language Models," *arXiv preprint arXiv:2404.06448*, Apr. 2024.
- [7] X. Chen, G. Zhu, H. Ding, L. Zhang, H. Zhang, and Y. Fang, "End-to-End Service Auction: A General Double Auction Mechanism for Edge Computing Services," *IEEE/ACM Trans. Networking*, vol. 30, no. 6, pp. 2616–2629, Jun. 2022.
- [8] X. Liu, Z. Yan, Y. Zhou, D. Wu, X. Chen, and J. H. Wang, "Optimizing Parameter Mixing Under Constrained Communications in Parallel Federated Learning," *IEEE/ACM Trans. Networking*, vol. 31, no. 6, pp. 2640–2652, Dec. 2023.
- [9] G. Qu, Z. Lin, F. Liu, X. Chen, and K. Huang, "TrimCaching: Parameter-sharing AI Model Caching in Wireless Edge Networks," *arXiv preprint arXiv:2405.03990*, May. 2024.
- [10] Y. Deng, X. Chen, G. Zhu, Y. Fang, Z. Chen, and X. Deng, "Actions at the Edge: Jointly Optimizing the Resources in Multi-access Edge Computing," *IEEE Wireless Commun.*, vol. 29, no. 2, pp. 192–198, Apr. 2022.
- [11] H. Yuan, Z. Chen, Z. Lin, J. Peng, Z. Fang, Y. Zhong, Z. Song, X. Wang, and Y. Gao, "Graph Learning for Multi-Satellite Based Spectrum Sensing," in *Proc. ICCT*, Oct. 2023.
- [12] X. Chen, G. Zhu, Y. Deng, and Y. Fang, "Federated Learning over Multihop Wireless Networks with In-network Aggregation," *IEEE Trans. Wireless Commun.*, vol. 21, no. 6, pp. 4622–4634, Apr. 2022.
- [13] B. McMahan, E. Moore, D. Ramage, S. Hampson, and B. A. y Arcas, "Communication-efficient Learning of Deep Networks From Decentralized Data," in *Proc. AISTATS*, Apr. 2017.
- [14] J. Konečný, H. B. McMahan, F. X. Yu, P. Richtárik, A. T. Suresh, and D. Bacon, "Federated Learning: Strategies for Improving Communication Efficiency," *arXiv preprint arXiv:1610.05492*, Oct. 2016.

- [15] Z. Lin, G. Qu, Q. Chen, X. Chen, Z. Chen, and K. Huang, "Pushing Large Language Models to the 6G Edge: Vision, Challenges, and Opportunities," *arXiv preprint arXiv:2309.16739*, Sep. 2023.
- [16] P. Vepakomma, O. Gupta, T. Swedish, and R. Raskar, "Split Learning for Health: Distributed Deep Learning without Sharing Raw Patient Data," *arXiv preprint arXiv:1812.00564*, Dec. 2018.
- [17] Z. Lin, G. Qu, X. Chen, and K. Huang, "Split Learning in 6G Edge Networks," *IEEE Wireless Commun.*, 2024.
- [18] S. Lyu, Z. Lin, G. Qu, X. Chen, X. Huang, and P. Li, "Optimal Resource Allocation for U-shaped Parallel Split Learning," *arXiv preprint arXiv:2308.08896*, Oct. 2023.
- [19] C. Thapa, P. C. M. Arachchige, S. Camtepe, and L. Sun, "SplitFed: When Federated Learning Meets Split Learning," in *Proc. AAAI*, Feb. 2022.
- [20] Huawei, *NET4AI: Supporting AI as a Service in 6G*. Cambridge, U.K.: Cambridge Univ. Press, Sep. 2022.
- [21] S. Wang, T. Tuor, T. Salonidis, K. K. Leung, C. Makaya, T. He, and K. Chan, "Adaptive Federated Learning in Resource Constrained Edge Computing Systems," *IEEE J. Sel. Areas Commun.*, vol. 37, no. 6, pp. 1205–1221, Mar. 2019.
- [22] X. Wu, F. Huang, Z. Hu, and H. Huang, "Faster Adaptive Federated Learning," in *Proc. AAAI*, Jun. 2023.
- [23] S. L. Smith, P.-J. Kindermans, and Q. V. Le, "Don't Decay the Learning Rate, Increase the Batch Size," in *Proc. ICLR*, Feb. 2018.
- [24] H. Yu and R. Jin, "On the Computation and Communication Complexity of Parallel SGD with Dynamic Batch Sizes for Stochastic Non-convex Optimization," in *Proc. ICML*, Jun. 2019.
- [25] T. Xiang, Y. Bi, X. Chen, Y. Liu, B. Wang, X. Shen, and X. Wang, "Federated Learning with Dynamic Epoch Adjustment and Collaborative Training in Mobile Edge Computing," *IEEE Trans. Mobile Comput.*, Jun. 2023.
- [26] W. Wu, M. Li, K. Qu, C. Zhou, X. Shen, W. Zhuang, X. Li, and W. Shi, "Split learning over Wireless Networks: Parallel Design and Resource Management," *IEEE J. Sel. Areas Commun.*, vol. 41, no. 4, pp. 1051–1066, Feb. 2023.
- [27] S. Wang, X. Zhang, H. Uchiyama, and H. Matsuda, "HiveMind: Towards Cellular Native Machine Learning Model Splitting," *IEEE J. Sel. Areas Commun.*, vol. 40, no. 2, pp. 626–640, Oct. 2021.
- [28] Z. Lin, G. Zhu, Y. Deng, X. Chen, Y. Gao, K. Huang, and Y. Fang, "Efficient Parallel Split Learning over Resource-constrained Wireless Edge Networks," *IEEE Trans. Mobile Comput.*, 2024.
- [29] D. Pasquini, G. Ateniese, and M. Bernaschi, "Unleashing the Tiger: Inference Attacks on Split Learning," in *Proc. CCS*, Nov. 2021.
- [30] Karimireddy, Sai Praneeth and Kale, Satyen and Mohri, Mehryar and Reddi, Sashank and Stich, Sebastian and Suresh, Ananda Theertha, "On the Convergence Properties of A K-step Averaging Stochastic Gradient Descent Algorithm for Nonconvex Optimization," in *Proc. IJCAI*, Jul. 2018.
- [31] H. Yu, R. Jin, and S. Yang, "On the Linear Speedup Analysis of Communication Efficient Momentum SGD For Distributed Non-convex Optimization," in *Proc. ICML*, Jun. 2019, pp. 7184–7193.
- [32] S. P. Karimireddy, S. Kale, M. Mohri, S. Reddi, S. Stich, and A. T. Suresh, "Scaffold: Stochastic Controlled Averaging for Federated Learning," in *Proc. ICLR*, Apr. 2020.
- [33] Y. Zhang, M. J. Wainwright, and J. C. Duchi, "Communication-efficient Algorithms for Statistical Optimization," in *Proc. NIPS*, Jun. 2012.
- [34] X. Lian, C. Zhang, H. Zhang, C.-J. Hsieh, W. Zhang, and J. Liu, "Can Decentralized Algorithms Outperform Centralized Algorithms? A Case Study for Decentralized Parallel Stochastic Gradient Descent," in *Proc. NIPS*, Jun. 2017.
- [35] H. Mania, X. Pan, D. Papailiopoulos, B. Recht, K. Ramchandran, and M. I. Jordan, "Perturbed Iterate Analysis for Asynchronous Stochastic Optimization," *SIAM J. Optim.*, vol. 27, no. 4, pp. 2202–2229, Jan. 2017.
- [36] T. Lin, S. U. Stich, K. K. Patel, and M. Jaggi, "Don't Use Large Mini-batches, Use Local SGD," in *Proc. ICLR*, Dec. 2019.
- [37] W. Shi, S. Zhou, Z. Niu, M. Jiang, and L. Geng, "Joint Device Scheduling and Resource Allocation for Latency Constrained Wireless Federated Learning," *IEEE Trans. Wireless Commun.*, vol. 20, no. 1, pp. 453–467, Sep. 2020.
- [38] W. Xia, W. Wen, K.-K. Wong, T. Q. Quek, J. Zhang, and H. Zhu, "Federated-learning-based Client Scheduling for Low-latency Wireless Communications," *IEEE Wireless Commun.*, vol. 28, no. 2, pp. 32–38, Apr. 2021.
- [39] W. Dinkelbach, "On Nonlinear Fractional Programming," *Manage. Sci.*, vol. 13, no. 7, pp. 492–498, Mar. 1967.
- [40] D. Yue and F. You, "A Reformulation-linearization Method for the Global Optimization of Large-scale Mixed-Integer Linear Fractional Programming Problems and Cyclic Scheduling aApplication," in *Proc. ACC*, Jun. 2013.
- [41] R. G. Ródenas, M. L. López, and D. Verastegui, "Extensions of Dinkelbach's Algorithm for Solving Non-linear Fractional Programming Problems," *Top*, vol. 7, pp. 33–70, Jun. 1999.
- [42] P. Tseng, "Convergence of A Block Coordinate Descent Method for Nondifferentiable Minimization," *J Optim Theory Appl.*, vol. 109, pp. 475–494, Jun. 2001.
- [43] A. Krizhevsky, G. Hinton *et al.*, "Learning Multiple Layers of Features From Tiny Images," *Tech. Rep.*, Apr. 2009.
- [44] Y. Lecun, L. Bottou, Y. Bengio, and P. Haffner, "Gradient-based Learning Applied to Document Recognition," *Proc. IEEE*, vol. 86, no. 11, pp. 2278–2324, Nov. 1998.
- [45] G. Zhu, Y. Wang, and K. Huang, "Broadband analog aggregation for low-latency federated edge learning," *IEEE Trans. Wireless Commun.*, vol. 19, no. 1, pp. 491–506, Oct. 2019.
- [46] Z. Yang, M. Chen, W. Saad, C. S. Hong, and M. Shikh-Bahaei, "Energy Efficient Federated Learning over Wireless Communication Networks," *IEEE Trans. Wireless Commun.*, vol. 20, no. 3, pp. 1935–1949, Nov. 2020.
- [47] Z. Lin, Z. Chen, Z. Fang, X. Chen, X. Wang, and Y. Gao, "FedSN: A General Federated Learning Framework over LEO Satellite Networks," *arXiv preprint arXiv:2311.01483*, Nov. 2023.
- [48] K. Simonyan and A. Zisserman, "Very Deep Convolutional Networks for Large-scale Image Recognition," in *Proc. ICLR*, 2015.